

# UCSF

## UC San Francisco Previously Published Works

### Title

Micrococcin cysteine-to-thiazole conversion through transient interactions between the scaffolding protein TcII and the modification enzymes TcIJ and TcIN.

### Permalink

<https://escholarship.org/uc/item/2d58s3q0>

### Authors

Calvopina-Chavez, Diana G

Burse, Devan M

Tseng, Yi-Jie

et al.

### Publication Date

2024-05-23

### DOI

10.1128/aem.00244-24

### Copyright Information

This work is made available under the terms of a Creative Commons Attribution License, available at <https://creativecommons.org/licenses/by/4.0/>

Peer reviewed

1     **Micrococцин cysteine-to-thiazole conversion through transient interactions**  
2             **between a scaffolding protein and two modification enzymes**

3  
4     Diana G Calvopina-Chavez<sup>1</sup>, Devan M Bursey<sup>1</sup>, Yi-Jie Tseng<sup>2</sup>, Leena M Patil<sup>2</sup>, Kathryn D  
5     Bewley<sup>3,4</sup>, Philip R Bennallack<sup>1,5</sup>, Josh M McPhie<sup>2</sup>, Kimberly B Wagstaff<sup>2</sup>, Anisha Daley<sup>2</sup>,  
6             Susan M Miller<sup>3</sup>, James D Moody<sup>2</sup>, John C Price<sup>2</sup>, \*Joel S Griffitts<sup>1</sup>

7  
8     <sup>1</sup>Department of Microbiology and Molecular Biology, Brigham Young University, Provo, UT  
9     84602

10  
11    <sup>2</sup>Department of Chemistry and Biochemistry, Brigham Young University, Provo, UT 84602

12  
13    <sup>3</sup>Department of Pharmaceutical Chemistry, University of California, San Francisco, CA 94143

14  
15    <sup>4</sup>Currently at: Genentech Inc, San Francisco, CA 94080

16  
17    <sup>5</sup>Currently at: Werfen North America, Bedford, MA 01730

18  
19    \*Correspondence should be addressed to J.S.G (email: joelg@byu.edu)

20  
21    Running Title: A scaffold protein coordinates cysteine to thiazole conversion

22  
23    Keywords: thiazole, thiopeptide, post-translationally modified peptides

## 24 ABSTRACT

25 Ribosomally synthesized and post-translationally modified peptides (RiPPs) are a broad group of  
26 compounds mediating microbial competition in nature. Azole/azoline heterocycle formation in  
27 the peptide backbone is a key step in the biosynthesis of many RiPPs. Heterocycle formation in  
28 RiPP precursors is often carried out by a scaffold protein, an ATP-dependent cyclodehydratase,  
29 and an FMN-dependent dehydrogenase. It has generally been assumed that the orchestration of  
30 these modifications is carried out by a stable complex including the scaffold, cyclodehydratase  
31 and dehydrogenase. The antimicrobial RiPP micrococcin begins as a precursor peptide (TcIE)  
32 with a 35-amino acid N-terminal leader and a 14-amino acid C-terminal core containing six Cys  
33 residues that are converted to thiazoles. The putative scaffold protein (TcII) presumably presents  
34 the TcIE substrate to a cyclodehydratase (TcIJ) and a dehydrogenase (TcIN) to accomplish the  
35 two-step installation of the six thiazoles. In this study, we identify a minimal TcIE leader region  
36 required for thiazole formation, we demonstrate complex formation between TcII, TcIJ and  
37 TcIN, and further define regions of these proteins required for complex formation. Our results  
38 point to a mechanism of thiazole installation in which TcII associates with the two enzymes in a  
39 mutually exclusive fashion, such that each enzyme competes for access to the peptide substrate  
40 in a dynamic equilibrium, thus ensuring complete modification of each Cys residue in the TcIE  
41 core.

42

## 43 IMPORTANCE

44 Thiopeptides are a family of antimicrobial peptides characterized for having sulfur-containing  
45 heterocycles and for being highly post-translationally modified. Numerous thiopeptides have  
46 been identified; almost all of which inhibit protein synthesis in gram-positive bacteria. These

47 intrinsic antimicrobial properties make thiopeptides promising candidates for the development of  
48 new antibiotics. The thiopeptide micrococcin is synthesized by the ribosome and undergoes  
49 several post-translational modifications (PTMs) to acquire its bioactivity. In this study, we  
50 identify key interactions within the enzymatic complex that carries out cysteine to thiazole  
51 conversion in the biosynthesis of micrococcin.

52

## 53 INTRODUCTION

54 Ribosomally synthesized and post-translationally modified peptides (RiPPs) are natural products  
55 produced by many bacteria that exhibit diverse biological activities including antimicrobial  
56 functions (1-6). RiPP biosynthesis starts with the ribosomal translation of a precursor peptide  
57 that is then heavily modified by multiple enzymes. The precursor peptide consists of an N-  
58 terminal leader sequence, also known as the recognition sequence, responsible for recruiting  
59 enzymes that carry out post-translational modifications (PTMs) (7-9), and a C-terminal core  
60 peptide sequence where PTMs occur (10-12). In most cases, RiPP biosynthetic gene clusters  
61 encode an E1-ubiquitin activating-like (E1-like) protein that has been implicated in leader  
62 peptide binding. This E1 homolog contains a RiPP recognition element (RRE) that adopts a  
63 highly conserved winged helix-turn-helix (wHTH) structure with three  $\alpha$ -helices and a three-  
64 stranded  $\beta$ -sheet. RiPP leader peptides bind to RRE domains by interacting at the interface of the  
65  $3\alpha/3\beta$  fold acting as a fourth  $\beta$  strand (13-15). After proper substrate recognition, numerous  
66 possible modifications take place on the core peptide culminating with the proteolytic removal of  
67 the leader from the core yielding a mature RiPP (7, 8).

68

69 Thiazole/oxazole-modified microcins (TOMMs) are a class of RiPPs that feature thiazol(in)e and  
70 oxazol(in)e heterocycles resulting from intramolecular reactions of cysteine, serine or threonine  
71 residues in the precursor peptide (16). Thiazole/oxazole biosynthesis is a two-step process in  
72 which an ATP-dependent cyclodehydratase (member of the YcaO superfamily) yields  
73 thiazoline/oxazoline heterocycles that are then oxidized into azoles by an FMN-dependent  
74 dehydrogenase. In addition to the cyclodehydratase and optional dehydrogenase, TOMM clusters  
75 encode proteins that facilitate coupling of the precursor peptide with these enzymes, but the  
76 different TOMM systems are highly variable in this respect. Most include an E1-like scaffold  
77 protein (mentioned above) and/or a second type of protein-protein interaction domain annotated  
78 as “Ocin-ThiF-like”. Either or both of these may contain an RRE, and the E1-like domain is  
79 often fused to the cyclodehydratase (17-23). This structural variability in TOMM complexes is  
80 illustrated in **Fig. 1**, which depicts four examples for which studies on the architecture of these  
81 complexes have been carried out. During biosynthesis of the cyanobactin trunkamide, the  
82 enzyme TruD catalyzes formation of azoline heterocycles. The crystal structure of TruD shows a  
83 fused cyclodehydratase with an NTD that contains an E1-like domain with an RRE, while the  
84 CTD comprises a YcaO domain responsible for catalyzing heterocycle formation (24, 25). The  
85 biosynthetic gene cluster for the bacteriocin heterocycloanthracin (HCA) contains a single copy  
86 of an Ocin-ThiF-like protein (HcaF), a fused E1-YcaO cyclodehydratase (HcaD), and a  
87 dehydrogenase (HcaB). In this system, the Ocin-ThiF-like protein interacts in a 1:1 ratio with the  
88 E1-like domain on the fused cyclodehydratase to yield azoline heterocycles. These azoline rings  
89 are then oxidized into azoles by a dedicated dehydrogenase, however, studies to characterize  
90 protein interactions with this enzyme have been unsuccessful (26, 27). For Microcin B17, the  
91 E1-like scaffold protein (McbB) interacts with a discrete cyclodehydratase (McbD) and a

92 dehydrogenase (McbC) in a higher order octameric complex with a ratio of 4:2:2 (22, 28). In a  
93 more complicated system, the biosynthetic gene cluster for the thiopeptide sulfomycin (Sul)  
94 encodes multiple copies of RREs (SulB, SulF), E1/Ocin-ThiF-like proteins (SulB, SulC, SulE,  
95 SulF), cyclodehydratases (SulC, SulD) and dehydrogenases (SulF, SulG). Combinations of these  
96 proteins form three complexes (SulBC, SuleFG, SulDEFG) that achieve Cys, Thr and Ser  
97 conversion into their corresponding thiazole, methyloxazole, and oxazole (23, 29). All these  
98 TOMM systems share certain biochemical features across a vast evolutionary distance, but they  
99 vary in their intersubunit architectures.

100

101 Micrococcin is a thiopeptide produced by several Gram-positive bacteria, including *Bacillus*  
102 *cereus* and *Macrococcus caseolyticus* (30-32). Its biosynthesis involves several PTMs, including  
103 thiazole formation, C-terminal decarboxylation, dehydroamino acid formation, and the creation  
104 of a pyridine-anchored macrocycle (33). The gene cluster responsible for micrococcin production  
105 in *M. caseolyticus* (**Fig. 2A**) is located on a plasmid and consists of 12 *tcl* genes, which is  
106 simpler than the 24-gene cluster found in *Bacillus cereus* (34, 35). Out of these 12 *tcl* genes, 8  
107 are essential for micrococcin production (31, 33). The roles of these genes are illustrated in **Fig.**  
108 **2B**. The precursor peptide for micrococcin, TcIE, has an N-terminal leader of 35 amino acids and  
109 a C-terminal core of 14 amino acids. Its biosynthesis begins with the conversion of all six  
110 cysteine residues in the core to thiazoles (31). Thiazole installation is required for all subsequent  
111 modifications (**Fig. 2B**). The work presented here focuses on the thiazole installation step in  
112 micrococcin biosynthesis. Each thiazole conversion is a two-step process requiring three  
113 proteins: a putative scaffold (TcII), a cyclodehydratase (TcIJ), and a dehydrogenase (TcIN) (**Fig.**  
114 **2C**). We have previously shown that in the absence of TcII, no formation of thiazolines or

115 thiazoles occurs, suggesting that this putative scaffold protein is essential for cys-to-thiazole  
116 conversion. When the TclJ cyclodehydratase is absent, there are no detectable thiazolines or  
117 thiazoles. In the absence of the TclN dehydrogenase, all six thiazoline heterocycles accumulate,  
118 suggesting that each Cys residue does not require complete modification before the next one is  
119 processed (31).

120

121 In this study, we investigate how the thiazole installation proteins in the micrococcin  
122 biosynthetic pathway interact with the substrate peptide, and with each other, to carry out these  
123 modifications. By conducting a truncation analysis on the TclE leader peptide sequence, we  
124 determined a 20-amino acid minimal recognition region required for thiazole installation.  
125 Furthermore, by using computational modeling and an *E. coli*-based expression system for  
126 mutagenesis and copurification experiments, we demonstrate complex formation between TcII,  
127 TclJ and TclN, and we propose a mechanism for cysteine to thiazole conversion in which the  
128 scaffold protein TcII coordinates thiazole installation by presenting the TclE substrate to each  
129 modifying enzyme in dynamic equilibrium.

130

## 131 RESULTS

### 132 **TclE, TcII, TclJ, and TclN can be functionally expressed in *E. coli***

133 We engineered a system in which *E. coli* would express codon-optimized *tcl* genes encoding  
134 TclE, TcII, TclJ, and TclN. Each of these was engineered with affinity tags in a manner which  
135 was previously shown to preserve functionality (31). To test the functionality of *E. coli*-  
136 expressed Tcl proteins, we evaluated the *in vitro* conversion of the six TclE Cys residues to  
137 heterocycles by mass spectrometry (**Fig. 3**). TclE was purified with an N-terminal cleavable GST

138 tag, and the three other TcI proteins were purified as complexes using N-terminally His-tagged  
139 TcII (these complexes are shown in figures below). In the absence of modifying enzymes, TcIE  
140 purification and proteolytic removal from the GST tag yields a leader-plus-core fragment of the  
141 expected molecular weight ( $m/z = 5373$ ). When treated with *E. coli*-produced TcII and TcIJ  
142 (TcIN excluded), TcIE resolved to two major peaks of  $m/z=5285$  and  $5266$ , consistent with the  
143 appearance of 5 and 6 thiazolines, respectively. When treated with *E. coli*-produced TcII, TcIJ  
144 and TcIN, the prominent TcIE product has  $m/z = 5253$ , consistent with the complete 6-thiazole  
145 product with an expected  $-120$  Da change ( $-6 \times (\text{H}_2\text{O}+2\text{H})$ ) compared to the unmodified peptide.

146

#### 147 **TcII<sub>NTD</sub> directly interacts with TcIE**

148 We hypothesized that TcII plays a role in TcIE recognition. Bioinformatic analysis using the  
149 program HHpred (36-38) indicates that TcII is structurally similar to Ocin-ThiF proteins. We  
150 obtained a structural model of the TcII:TcIE dimer using AlphaFold2 (**Fig. 4A**). The TcII model  
151 contains two distinct domains, the N-terminal domain (NTD) is a wHTH structure comprised of  
152 three  $\alpha$  helices and three  $\beta$  strands, consistent with an RRE. This model places TcIE at the  
153 interface between the  $\alpha$  helices and the 3-stranded  $\beta$  sheet with the leader sequence acting as a  
154 fourth  $\beta$  strand, similar to what has been shown for crystallography solved structures in other  
155 TOMM systems (20, 22, 24). Key TcIE residues in this interaction start with F17 occupying a  
156 hydrophobic pocket at the interface of TcII helix 3 and  $\beta 3$ . Other predicted key interactions  
157 between the TcIE leader and the TcII RRE involve three salt bridges: TcIE(E21)-TcII(K31),  
158 TcIE(E22)-TcII(K78), and TcIE(E28)-TcII(K22) (**Fig. 4A**). To further investigate whether the  
159 TcII<sub>NTD</sub> is an RRE, we tested for TcII<sub>NTD</sub> binding to TcIE by copurification. We co-expressed  
160 His-tagged TcII<sub>NTD</sub> (residues 1-85) with GST-tagged TcIE in *E. coli* and carried out



161 copurification with nickel-NTA beads. As shown in **Figure 4B**, TcII<sub>NTD</sub> pulls down TcIE (**Fig.**  
162 **4B, Lane 3**), indicating a non-covalent interaction between the two proteins. Furthermore,  
163 TcII<sub>NTD</sub> copurifies the TcIE leader region when the TcIE core region is absent (**Fig. S1**). We then  
164 attempted to determine a minimal TcIE leader that interacts with TcII<sub>NTD</sub>, so we generated a  
165 series of leader truncations in which 3 residues were consecutively removed from the N-terminus  
166 of TcIE (**Fig. 5A**) for a total of six TcIE truncation variants:  $\Delta 3$ ,  $\Delta 6$ ,  $\Delta 9$ ,  $\Delta 12$ ,  $\Delta 15$ , and  $\Delta 18$ . Each  
167 truncated variant was co-expressed with His-tagged TcII<sub>NTD</sub>, and nickel pull-down experiments  
168 were carried out. As shown in **Figure 5B**, some copurification could be detected for all TcIE  
169 truncations, but the interaction appears weakened beyond the  $\Delta 9$  truncation. We observe that, as  
170 more of TcIE is removed, the amount of TcII<sub>NTD</sub> purified becomes less. This suggests that the  
171 stability of this putative RRE domain is enhanced by the presence of a fully functional leader  
172 peptide.

173

#### 174 **Determination of a functionally minimal TcIE leader peptide**

175 We then used the TcIE truncation series to investigate leader sequence requirements for thiazole  
176 installation in *E. coli* cells co-expressing TcII, TcIJ, and TcIN. We used four of the TcIE  
177 truncated variants ( $\Delta 9$ ,  $\Delta 12$ ,  $\Delta 15$ , and  $\Delta 18$ ) and assessed thiazole installation by Orbitrap liquid  
178 chromatography mass spectrometry (LC-MS) after GST-TcIE purification from co-expressing  
179 cells (**Fig. 6**). For this analysis, we define “fully modified peptides” as those in which all Cys  
180 residues are converted to thiazoles. For the  $\Delta 9$  truncation 100% of detected TcIE peptides were  
181 fully modified. The  $\Delta 12$  variant also yielded products consistent with having a fully modified  
182 core, while the  $\Delta 15$  variant produced a slightly reduced yield of fully modified product (mean=  
183  $99.8 \pm 0.2\%$ ; n=3), with some detected peptides containing intermediates with 4-5 thiazoles. The

184  $\Delta 18$  leader truncation yielded multiple intermediates containing a combination of thiazoles,  
185 thiazolines and cysteines. The mean of fully modified TcIE with the  $\Delta 18$  truncation is  $71.6 \pm$   
186  $4.8\%$  ( $n=3$ ). We conclude from this that the first 12 N-terminal amino acids of TcIE are not  
187 required for thiazole installation, and amino acids 12-15 have minimal impact. When amino  
188 acids 15-18 are removed, it significantly impairs thiazole installation, potentially due to loss of  
189 key TcIE-RRE non-covalent interactions (see Fig. 4A). Recall that TcIE(F17) was already  
190 predicted to mediate an important interaction in a hydrophobic pocket of the modeled TcII<sub>NTD</sub>.  
191 Previous studies with TOMM systems such as streptolysin and microcin B17 have shown that  
192 the leader peptide is primarily engaged through a conserved FXXXB (B= V, I, or L) motif (39,  
193 40). The TcIE leader contains a similar motif (FXXXXB) in residues 17-22. The convergence of  
194 these empirical findings with the AlphaFold2 structural prediction and these observations in  
195 other TOMM systems gives credibility to a model in which the TcII<sub>NTD</sub> functions as a genuine  
196 RRE in micrococcin biosynthesis.

197

### 198 **TcII<sub>CTD</sub> binds to TcIJ and TcIN**

199 Given that TcII<sub>NTD</sub> engages with TcIE, we hypothesized that the C-terminal domain (CTD) of  
200 TcII may be primarily involved in recruiting the enzymatic proteins TcIJ and TcIN. Ocin-ThiF  
201 proteins like TcII have previously been shown to mediate interactions with TOMM enzymes (3,  
202 23, 26). To test interactions of full-length TcII to the modifying enzymes, we co-expressed His-  
203 tagged TcII with TcIJ or with TcIN in *E. coli* and carried out nickel copurification experiments.  
204 As shown in **Figure 7** (Lane 3), TcII interacts with both TcIJ and TcIN when all three proteins  
205 are expressed together. When co-expressed with each individual enzyme, TcII also copurifies  
206 them (**Fig. 7, Lanes 4-5**). His-tagged TcII<sub>CTD</sub> (residues 85-242) also copurifies TcIJ and TcIN

207 **(Fig. 7, lane 7-8)**, though TcII<sub>CTD</sub>:TclN shows a weaker interaction than TcII<sub>CTD</sub>:TclJ. These  
208 results point to TcII<sub>CTD</sub> as being sufficient for binding to both TclJ and TclN.  
209  
210 Initially, we interpreted these results to mean that TcII has two unique interaction surfaces on its  
211 CTD, simultaneously recruiting TclJ and TclN as a stable enzymatic complex. To test whether  
212 the TcIIJN proteins form a ternary stable complex, we carried out copurification experiments  
213 with varying tagging arrangements. We created nine strains expressing different combinations of  
214 His-tagged TcII, TclJ and TclN. These experiments show that TcII copurifies TclJ and TclN  
215 regardless of whether TcII is N-terminally or C-terminally His-tagged **(Fig. 8, Lanes 2-3)**,  
216 although TcII may be more poorly expressed or less stable when C-terminally tagged.  
217 Furthermore, TcII binding to TclJ appears to be favored when TcII is C-terminally tagged. N-  
218 terminally tagged TclJ does not copurify any detectable amounts of TcII or TclN **(Fig. 8, Lane**  
219 **4)**; however, when the tag is moved to the TclJ C-terminus, TclJ robustly pulls down TcII, with  
220 little evidence of TclN copurifying **(Fig. 8, Lane 5)**. When an N-terminal region of  
221 TclJ (residues 1-115) is C-terminally tagged, it very robustly copurifies TcII, and a minor band  
222 consistent with TclN can be observed **(Fig. 8, Lane 6)**. TclN strongly copurifies TcII regardless  
223 of the location of the tag **(Fig. 8, Lanes 8-9)**, with possibly a minor TclJ copurification product.  
224 In all cases where TcII is pulled down by a tagged version of TclJ or TclN, the band intensities  
225 indicate a stoichiometric excess of TcII ranging from 2 to 8 based on densitometry that accounts  
226 for staining intensity and molecular weight. In all cases where TcII is pulled down by either  
227 tagged enzyme, copurification of the untagged other enzyme is absent or barely evident. From  
228 these overall results, we hypothesize that TcII engages with TclJ and TclN in a competitive  
229 fashion, and that there may be a weak interaction between the two enzymes.

230

231 **One surface of TcII facilitates binding to TcIJ and TcIN**

232 We generated structural models of TcII:TcIJ and TcII:TcIN dimers using AlphaFold2 (**Fig. 9A,**  
233 **9B**). According to these two models, TcII<sub>NTD</sub> folds in a similar conformation for both, while  
234 TcII<sub>CTD</sub> takes on a slightly different structure in each predicted complex, with Helix 6 (TcII  
235 residues 188-213) being a central structure for binding to both enzymes. These models reinforce  
236 the notion that the TcII:TcIJ and TcII:TcIN complexes are alternative and mutually exclusive  
237 structures. To investigate whether Helix 6 is the primary interaction surface of TcII for binding to  
238 the enzymes, we genetically dissected the region corresponding to Helix 6 by substituting each  
239 of its 15 surface-exposed residues with an arginine residue and tested for binding to TcIJ and  
240 TcIN under the same conditions used for the copurification shown in **Fig. 8** Lane 2. For this, 15  
241 *E. coli* strains were constructed that express TcIJ, TcIN and His-tagged TcII with its  
242 corresponding Helix 6 substitutions (**Fig. S2**). Copurification experiments show that TcII  
243 residues Y189, I198, I202, and T212 are important for the TcII:TcIJ interaction since these Arg  
244 substitutions abolish binding interactions between the two proteins (**Fig. 10A, Lanes 2, 4, 6, 10**).  
245 TcII residues H194, N201, S205, F208, and L209 are critical for interaction with TcIN, as when  
246 these residues are substituted, TcII:TcIN interactions are disrupted (**Fig. 10A, Lanes 3, 5, 7, 8,**  
247 **9**). Substitutions T188, L197, C199, E206, Y210, and S213 had no effect in TcII interactions  
248 with either TcIJ or TcIN (**see Fig. 10B; Fig. S2**). Substitutions T212R and F208R resulted in a  
249 weaker TcII band, suggesting that these changes may also have a negative effect on TcII folding  
250 or stability. These findings indicate that Helix 6 is a pivotal structure within TcII responsible for  
251 recruiting both TcIJ and TcIN. Key residues of Helix 6 facilitating binding to each enzyme are

252 interspersed within this postulated surface of TcII<sub>CTD</sub>, further supporting the notion of two  
253 enzymes competing for one TcII docking site.

254

### 255 **An independent domain of TcIJ facilitates binding to TcII**

256 We wanted to further investigate how the N-terminal region of TcIJ (when C-terminally tagged),  
257 is able to pull down TcII, while the N-terminally tagged full-length TcIJ is unable to (see **Fig. 8,**  
258 **Lanes 4-5**). We reasoned that the N-terminus of full-length TcIJ is important for TcII interaction.  
259 We obtained AlphaFold2 models of TcIJ and TcIN (**Fig. S3A, and S3B**). The TcIJ model  
260 features two distinct domains, corresponding to a small NTD (residues 1-105) with the enzyme  
261 active site in a larger YcaO-like CTD (residues 115-242). HHpred analysis showed that the NTD  
262 of TcIJ is a short E1-like domain likely involved in protein-protein interactions. The TcIJ C-  
263 terminus is embedded in its putative active site, while its N-terminus is predicted to be surface  
264 exposed on this E1-like NTD. We hypothesized that TcIJ<sub>NTD</sub> folds independently and facilitates  
265 binding to TcII. To test this, two versions of the TcIJ<sub>NTD</sub> (residues 1-105 and residues 1-115) were  
266 co-expressed with His-tagged TcII for nickel copurification. Both versions of TcIJ<sub>NTD</sub> copurified  
267 with TcII (**Fig. 11, Lanes 3-4**) indicating that the E1-like domain of TcIJ (residues 1-105) folds  
268 independently and forms a TcII-binding domain. Tags on the N-terminus of this domain appear  
269 to obstruct TcII binding (see **Fig. 8, Lane 4**).

270

### 271 **Analysis of TcIIJN complexes by size-exclusion chromatography**

272 To investigate this model, we evaluated the TcIIJN complexes using size-exclusion  
273 chromatography. We first established the oligomeric state of purified TcII, which was consistent  
274 with a monomer (**Fig. 12**). However, when TcII, TcIJ and TcIN were analyzed as a mixture, a

275 new peak arose with a retention time consistent with a molecular weight of ~120 kDa, suggesting  
276 molecular units that contain two copies of TcII and one copy of either enzyme (2TcII:1TcIJ,  
277 expected: 121 kDa or 2TcII:1TcIN, expected: 111 kDa) (**Fig. 12**).

278

## 279 DISCUSSION

280 The TcI biosynthetic pathway from *M. caseolyticus* synthesizes micrococcin from a precursor  
281 peptide (TcIE) by orchestrating the following post-translational modifications: Cys-to-thiazole  
282 conversion, C-terminal decarboxylation, Ser/Thr dehydration, and macrocyclization. The work  
283 provided in this study focuses on the thiazole installation step to provide a better understanding  
284 of the complex protein interactions of thiazole modifying enzymatic proteins. Thiazole  
285 installation occurs in a two-step process in which a cyclodehydratase (TcIJ) converts six  
286 cysteines in the core peptide of TcIE into thiazolines, and then a dehydrogenase (TcIN) converts  
287 the thiazolines into thiazoles. In this study, we determined a minimal region on the leader peptide  
288 that is required for thiazole installation, we show complex formation between TcII, TcIJ, and  
289 TcIN, and further define conserved domains within these proteins that play a critical role  
290 mediating protein interactions for cysteine to thiazole conversion.

291

292 Thiazole/oxazole modified microcins (TOMMs) are derived from a precursor peptide that  
293 contains an N-terminal leader and a C-terminal core. Modifications in TOMM precursor peptides  
294 are orchestrated by an E1-like scaffold protein, a YcaO cyclodehydratase, and a dehydrogenase;  
295 in some cases, a highly divergent Ocin-ThiF-like protein is also present (16, 21, 26, 41, 42). The  
296 E1-like and Ocin-ThiF-like proteins are involved with leader peptide binding through an RRE  
297 domain that features a winged helix-turn-helix (wHTH) structure comprised of three  $\alpha$ -helices

298 and a three-stranded  $\beta$ -sheet (15). The purpose of the leader peptide is to recruit the biosynthetic  
299 enzymes, but they have shown variations in their roles in the biosynthesis of diverse TOMMs  
300 (20, 43-45). For instance, studies in Lantibiotics such as Nisin have shown that the core can be  
301 processed in the absence of the leader peptide, albeit with reduced efficiency (46, 47). Reports  
302 for cyanobactin processing by LynD have shown that in the absence of the leader, the core does  
303 not get modified; however, if the leader is provided as a separate peptide (*in trans*) or appended  
304 to the N-terminus of the biosynthetic enzyme, the substrate is fully modified (20, 43, 48). In this  
305 study, we define the NTD of TcII as the RRE that directly interacts with the TcIE leader, and we  
306 define a minimal leader region that is essential for binding to the RRE and allows for complete  
307 thiazole installation by the biosynthetic enzymes. Reports on streptolysin and microcin B17 have  
308 determined that the leader peptide is recognized by a conserved FXXXB (B= V, I, or L) motif  
309 (39, 40). Our studies show that truncation of a similar motif (FXXXXB) in the TcIE leader  
310 significantly reduces RRE binding and thiazole installation. This suggest a shared strategy in the  
311 leader of TOMM precursors that has been conserved through evolutionary timescale.

312  
313 TOMM biosynthetic clusters have shown a wide variety of structural variations in how the  
314 biosynthetic enzymes interact with each other to install azole heterocycles onto a precursor  
315 peptide. The solved structures of the TruD and LynD cyclodehydratases provide an example of  
316 fused cyclodehydratases that contain an E1-like and a YcaO domain (49, 50). TOMM proteins  
317 for the Heterocycloanthracin (Hca) biosynthetic cluster feature a single copy of an Ocin-ThiF-  
318 like protein (HcaF), a fused E1-YcaO cyclodehydratase (HcaD), and a dehydrogenase (HcaB),  
319 with the Ocin-ThiF-like protein comprising of an RRE and interacting in a 1:1 ratio with the  
320 fused cyclodehydratase; attempts to elucidate interactions between the scaffold protein and the

321 dehydrogenase for the Hca pathway have not been possible because the dehydrogenase is heavily  
322 proteolyzed when expressed in *E. coli* (26). The Microcin B17 synthetase features a discrete  
323 cyclodehydratase (McbD) and dehydrogenase (McbC) that are dependent on the presence of an  
324 E1-like protein (McbB) for substrate recognition forming a higher order active complex with a  
325 ratio of 4McbB:2McbD:2McbC (22). The TOMM proteins for the biosynthesis of sulfomycin  
326 feature combinations of RREs (SulB, SulF), E1/Ocin-ThiF-like domains (SulB, SulC, SulE,  
327 SulF), cyclodehydratases (SulC, SulD) and dehydrogenases (SulF, SulG). Combinations of these  
328 proteins form three active complexes (SulBC, SulEFG, SulDEFG) that achieve azole formation  
329 in the substrate peptide (23). Our findings show that the TOMM proteins from the Tcl  
330 biosynthetic cluster comprise of an Ocin-ThiF-like protein (TclI) that includes an RRE, a fused  
331 cyclodehydratase (TclJ) that includes an E1-like domain and a YcaO domain, and a  
332 dehydrogenase (TclN). TclI binds to the TcIE leader through its RRE and presents the core  
333 peptide to each enzyme in a mutually exclusive manner, forming two distinct complexes  
334 (TclI:TclJ, and TclI:TclN). Our results also suggest that the enzymes may interact weakly with  
335 each other creating spatial constraints, so that both enzymes are readily available to bind to TclI  
336 when taking turns to modify TcIE in a coordinated manner (**Fig. 13**).

337

338 Size exclusion chromatography data suggests that TclI exists in a monomeric conformation when  
339 expressed by itself, but it adopts a homodimeric structure when interacting with the enzymes  
340 (**Fig. 12**). Furthermore, preliminary copurification experiments (**Fig. S4**) suggest that TclI may  
341 indeed form a homodimer, thus the ratio of the active complexes might consist of 2TclI:1TclJ,  
342 and 2TclI:1TclN, but further investigation is required to validate this claim. Overall, the findings  
343 from this study have not only elucidated key domains of TOMM proteins in the Tcl biosynthetic



344 cluster, but it provides evidence of the high functional and structural diversity of the TOMM  
345 protein family.

346

## 347 MATERIALS AND METHODS

### 348 **Plasmids, strains, and culture conditions**

349 The bacterial strains and plasmids used in this study are summarized in Tables S1 and S2. For  
350 full plasmid sequences, refer to the Supplemental Materials file. Plasmids were constructed and  
351 maintained in *E. coli* strain DH5 $\alpha$ . The *tcl* genes were synthesized with codon optimization for  
352 expression in *E. coli*. The sequences of vectors and *tcl* gene inserts are given in the supplemental  
353 information file. For protein expression, plasmids were transformed into strain BL21, Nico 21  
354 (DE3) or DH5 $\alpha$ . All bacterial cultures were grown in Luria broth (LB: per liter, 10 g Bacto  
355 tryptone, 5 g Bacto yeast extract, 5 g NaCl, 1 ml 2N NaOH). Antibiotics used were kanamycin  
356 (30  $\mu$ g/ml), ampicillin (100  $\mu$ g/ml), and chloramphenicol (30  $\mu$ g/ml). Cultures were induced for  
357 protein expression using 0.3 mM isopropyl  $\beta$ -D-1-thiogalactopyranoside (IPTG).

358

### 359 **Tcl protein expression and purification**

360 To prepare samples for SDS-PAGE analysis, overnight liquid cultures (4 ml) were grown from  
361 single colonies in the presence of appropriate antibiotics. 50-ml cultures were inoculated with 2  
362 ml of overnight culture, allowed to grow at 30°C for 1 h, followed by induction with IPTG for  
363 another 6 h at 30°C. Cells were collected by centrifuging the culture, and cell pellets were frozen  
364 at -80°C for a minimum of 1 h. Cell pellets were then processed for protein purification with  
365 either Ni-NTA-linked (for the His<sub>6</sub> tag) or glutathione-linked (for the GST tag) resin, as detailed  
366 below.

367

368 For His purification, cell pellets were thawed on ice and re-suspended in 1 ml of lysis buffer (50  
369 mM HEPES pH 7.8, 300 mM NaCl, 0.2 % Triton X-100, 0.5 mg/ml lysozyme, 60  
370 mM imidazole, 1 mM EDTA). Lysis took place for 1 h at 4°C. Cell lysates were then sonicated 4  
371 × 20 sec using a probe sonicator to ensure complete lysis and fragmentation of DNA. Samples  
372 were centrifuged at 13,000 rpm for 10 min (4°C) and approximately 1 ml of supernatant was  
373 transferred to a new microcentrifuge tube. Supernatant was incubated end-over-end with 50 µl of  
374 NTA-nickel agarose beads (Qiagen) at 4°C for 30 min. Nickel beads were pelleted at 13,000 rpm  
375 for 30 seconds and washed 3 × 1 ml with wash buffer (60 mM imidazole, 300 mM NaCl, 50 mM  
376 HEPES pH 7.8). Purified proteins were then eluted in 50 µl of 2x SDS sample buffer (20%  
377 glycerol, 83 mM Tris pH 6.8, 40 mg/ml sodium dodecyl sulfate (SDS), 0.01% bromophenol  
378 blue, 0.03 µl/ml 2-mercaptoethanol).

379 For GST purifications, cell pellets were thawed on ice and re-suspended in 1 ml lysis buffer (50  
380 mM Tris 8.0, 150 mM NaCl, 0.5 mg/ml lysozyme, 2 mM EDTA, and 0.2% Triton X-100). Cells  
381 were lysed for 1 h at 4°C then dithiothreitol (DTT) was added to a final concentration of 1.5  
382 mM. Samples were sonicated 4 × 20 sec. Cell lysates were centrifuged at 13,000 rpm at 4°C for  
383 10 min to pellet cell debris. Approximately 1 ml of supernatant was transferred to a new  
384 microcentrifuge tube. 50 µl of unwashed glutathione-agarose beads was added and samples were  
385 rotated end over end for 45 min at 4°C. Slurry was pelleted at 13,000 rpm for 30 seconds.  
386 Supernatant was removed and beads were washed 3 × 1 ml GST buffer (50 mM Tris 8.0, 150  
387 mM NaCl). GST buffer was completely removed, and proteins were eluted from resin in 50 µl of  
388 2x SDS sample buffer.

389

390 Purified samples were heated at 100°C for 5 min. Unless stated otherwise, 8 µl of supernatant  
391 was loaded onto a 12% resolving Laemmli gel with a 4% stacking gel. Gels were run using 1x  
392 Laemmli running buffer, stained overnight in coomassie blue stain, followed by destaining and  
393 soaking in water prior to imaging.

394

### 395 **Mass spectrometry analysis of TcIE processing**

396 For purification of His<sub>6</sub>-tagged enzymes for mass spectrometry analysis, 25-ml overnight  
397 cultures were grown from single colonies. These overnight cultures were then used to inoculate 1  
398 L induction cultures (30°C). After 1 h, IPTG was added and the cultures were grown for an  
399 additional 6 hours. The cells were harvested by centrifugation and the cell pellets were frozen at  
400 -80°C overnight. For copurification of His<sub>6</sub>-TcIIJ, His<sub>6</sub>-TcIIN, or His<sub>6</sub>-TcIIJN the cells were then  
401 thawed on ice with the addition of lysis buffer (50 mM HEPES, 150 mM NaCl, pH 7.8). A  
402 protease inhibitor tablet (Roche), 0.2% Triton X-100 and 0.5 mg/ml lysozyme were added and  
403 the cells were incubated on ice for 1 h. Complete lysis was achieved by sonication for 2 min on  
404 ice using a Branson Sonifier 450, followed by centrifugation for 20 min at 32,539 × g. The  
405 supernatant was incubated with 1 ml of Talon resin for 30 min at 4°C. Resin was washed with 3  
406 × 10 ml lysis buffer, followed by elution with lysis buffer plus 75 mM imidazole (4 × 1 ml). The  
407 elution fractions containing protein were buffer exchanged back into lysis buffer, concentrated,  
408 flash frozen with 10% glycerol, and stored at -80°C.

409

410 For purification of GST-tagged TcIE, 30-ml cultures were inoculated with 1 ml overnight  
411 culture, grown at 37°C until an OD<sub>600</sub> = 0.6, then IPTG was added and the cells were grown for  
412 an additional 20 h at 25°C. The cells were harvested by centrifugation and the cell pellets were

413 frozen at  $-80^{\circ}\text{C}$  for at least 30 min. The cells were then thawed and resuspended in 1 ml lysis  
414 buffer (50 mM Tris pH 8, 150 mM NaCl, 0.5 mg/ml lysozyme, 2 mM EDTA and one Roche  
415 protease inhibitor tablet per 10 ml). Complete lysis was achieved after a 15-min incubation at  
416 room temperature, followed by addition of DTT to 1.5 mM. Lysate was processed with several  
417 short sonication pulses with a microtip. Insoluble material was centrifuged at  $7,000 \times g$ , and the  
418 supernatant was combined with 30  $\mu\text{l}$  of glutathione-agarose resin (slurry) at  $4^{\circ}\text{C}$  for 45 min  
419 (rotating). The resin was pelleted and the beads were washed with GST buffer three times and  
420 the peptide was eluted with 40  $\mu\text{l}$  GST buffer plus 10 mM reduced glutathione. The eluant was  
421 either frozen at  $-80^{\circ}\text{C}$  for later use, or directly treated with tobacco etch virus (TEV) protease  
422 and ZipTipped (using the manufacturer's instructions).

423 Activity of TcI enzymes was tested *in vitro*. 20- $\mu\text{l}$  reactions containing 20  $\mu\text{M}$  GST-TcIE, 5 mM  
424 DTT, 2 mM ATP, 20 mM  $\text{MgCl}_2$ , 1  $\mu\text{M}$  enzymes, and 1  $\mu\text{g}$  TEV protease, were allowed to react  
425 for 40 min at RT. Reactions were zip-tipped (using the manufacturer's instructions) and analyzed  
426 by matrix-assisted laser desorption ionization-time of flight (MALDI-TOF) mass spectrometry.

427

#### 428 **Orbitrap Liquid Chromatography Mass Spectrometry (LC-MS) for TcIE truncation series**

429 GST-TcIE leader-truncated samples were co-expressed with TcIIJN as described in the TcI  
430 protein expression and purification section. GST-TcIE leader truncations were purified using  
431 glutathione beads as described above and TcIE peptides were removed from the GST tag through  
432 TEV protease cleavage. Truncated TcIE peptide samples were alkylated to cap any reduced  
433 cysteines using chloroacetamide at 20 mM. The peptides were then separated and measured via  
434 liquid chromatography-mass spectrometry (LC-MS) on an Easy nLC 1200 in connection with a  
435 Thermo Easy-spray source and an Orbitrap Fusion Lumos. Peptides were pre-concentrated with

436 buffer A (3% acetonitrile, 0.1% formic acid) onto a PepMap Neo Trap Cartridge (particle size 5  
437  $\mu\text{m}$ , inner diameter 300  $\mu\text{m}$ , length 5 mm) and separated with an EASY-Spray™ HPLC Column  
438 (particle size 2  $\mu\text{m}$ , inner diameter 75  $\mu\text{m}$ , length 25 mm) with increasing buffer B (80%  
439 acetonitrile, 0.1% formic acid) gradient:

440 Samples were eluted using a gradient of 5% B to 22% B over 85 minutes (128 minutes for  
441 muscle), 22% to 32% B over 15 minutes (22 minutes for muscle), with a wash of 32% to 95% B  
442 over 15 minutes, which was held at 95% B for 15 minutes followed by a wash step consisting of  
443 two washes going from 95% B to 2% B over 3 minutes, holding at 2% B for 3 minutes, returning  
444 to 95% over 3 minutes and holding for 3 minutes were performed. Sample loading and  
445 equilibration were performed using the HPLC's built in methods. LC-MS only runs were  
446 performed using 2400 V in the ion source, scan range of 375-1700 m/z, 30% RF Lens,  
447 Quadrupole Isolation, 8 \*105 AGC Target and a maximum injection time of 50 ms. The MS-  
448 based data-dependent acquisition method was set to a 3 second cycle time. MS1 scans were  
449 acquired by the orbitrap at a resolution of 120,000. Precursors with a charge > 1 and < 6 were  
450 selected for MS2 fragmentation. MS2 scans of CID precursor fragments were detected with the  
451 linear ion trap at a scan rate of 33.333 Da/sec with a Dynamic injection time. CID collisions  
452 were set to 30% for 10ms. After 3 selections a 60 second dynamic exclusion window was  
453 enabled; isotopes and unassigned charge states were excluded.

454

#### 455 **Data Processing for Label-free Quantitation**

456 Raw files were searched against a FASTA data base for the TCL operon (containing I, J, N, and  
457 E entries) with the *E. coli* proteome as a contaminant (Uniprot Reference UP000000625) using  
458 Peaks Studio analysis. The parent mass error tolerance was set to 10 ppm and the fragment mass

459 error tolerance was set to 0.5 Da. Cysteine carbamidomethylation, thiazoline, and thiazole were  
460 set as a variable modification, as well as methionine oxidation and pyro-glu from glutamine were  
461 set as variable modifications in the search. Digest mode was set to unspecific, and the peptide  
462 length range was set to 6 – 55 amino acids. The false discovery rate (FDR) for peptide matches  
463 was set to 1%, and protein ID significance was set to  $-10\log(\text{P-value}) \geq 15$ . Label-free data was  
464 normalized using the TIC option in PEAKS then the total signal for the modified form was  
465 compared as a fraction of the total signal for the peptide of interest (**File S1**).

466

467

468

#### 469 **Modeling and optimization of TcI protein structures**

470 The sequences of TcII, TcIJ, TcIN, as well as the protein hetero-dimers such as TcIE:TcII,  
471 TcII:TcIJ and TcII:TcIN were submitted online to the AlphaFold2 Google colab (51, 52) for  
472 structural predictions. The top-ranked models were selected for each TcI protein and dimer. Each  
473 model underwent optimization using the FastRelax algorithm (53) within PyRosetta. Energy  
474 calculations for each model were carried out using the ref2015 score function (54, 55) in  
475 PyRosetta. Binding energies were determined by subtracting the energies of the bound and  
476 unbound state models. Additionally, to assess the binding modes, we calculated the shape  
477 complementarities (56) of the complex models using Python logic and PyRosetta. These models  
478 were visualized using PyMOL, and a list of interacting residues (L187R, T188R, Y189R,  
479 H194R, I198R, C199R, N201R, I202R, S205R, E206R, F208R, L209R, Y210R, T212R, S213R)  
480 was identified for use in mutagenesis experiments.

481

482 **Size Exclusion Chromatography of TcII and TcIIJN complex**

483 Purified complex was filtered through 0.2  $\mu\text{m}$  cellulose filter (14000 g, 2 min). All the samples  
484 were vacuum dried, and then resuspended in SEC buffer (100 mM sodium phosphate with pH  
485 6.8, 0.023%  $\text{NaN}_3$ ) to make the final concentration to 1  $\mu\text{g}/\mu\text{L}$ . The Agilent 1260 Infinity HPLC  
486 System (Agilent, Santa Clara, CA) equipped with quaternary pump, manual injector,  
487 thermostatted column compartment, diode array detector (DAD) was used to carry out the  
488 analytical size exclusion chromatography. A Yarra-1.8  $\mu\text{m}$  X 150 $\text{\AA}$ , 150 x 4.6 mm HPLC  
489 column (00F-4631-E0, Phenomenex, USA) was used for separation of molecules. The Agilent  
490 system and column were equilibrated with 100 mM Sodium Phosphate with pH 6.8, 0.023%  
491  $\text{NaN}_3$  at a flow rate of 0.3 mL/min at 25  $^\circ\text{C}$ . The molecular weight calibration curve for SEC was  
492 obtained by running a protein standard mix containing bovine thyroglobulin (670 kDa), IgA  
493 (300 kDa), IgG (150 kDa), ovalbumin (44 kDa), myoglobin (17 kDa) and uridine (0.244 kDa),  
494 (AL0-3042, Phenomenex, CA, USA) to relate the molecule's size to elution volume. The  
495 injection volume for the protein standard and the protein samples was 5  $\mu\text{L}$ , and the elution  
496 volume was measured using the UV detector. All the data was collected at 280 nm, with a  
497 reference wavelength of 600 nm.

498

499 **Bioinformatics analysis of E1/YcaO, and Ocin-ThiF-like domains**

500 Protein sequences of TcII and TcIJ were submitted to HHpred (36-38) in FASTA format using  
501 standard parameters, and PDB70 and TIGRFAMs databases to analyze for the presence of  
502 E1/YcaO/Ocin-ThiF-like domains using pairwise comparison of profile HMM (hidden Markov  
503 model). The results of this analysis provided a list of known homologs with well-defined

504 domains, and multiple sequence alignments that were used to define each domain on the TcII and  
505 TcIJ proteins.

506

## 507 ACKNOWLEDGEMENTS

508 Research reported in this publication was supported by the National Institutes of Health (NIH)  
509 grants 1R15GM132852-01 to JSG and R01AG066874 to JCP. We thank Clarissa Clark and  
510 Katherine Brown for their assistance in processing samples for Liquid Chromatography Mass  
511 Spectrometry and Size Exclusion Chromatography.

512

513

## 514 REFERENCES

- 515 1. Kelly WL, Pan L, Li C. Thiostrepton biosynthesis: prototype for a new family of  
516 bacteriocins. *J Am Chem Soc.* 2009;131(12):4327-34.
- 517 2. Kutscher AH, Seguin L, Zegarelli EV, Piro JD. Antimicrobial activity of thiostrepton:  
518 tube dilution studies. *J Am Dent Assoc.* 1959;59:715-20.
- 519 3. Benazet F, Cartier M, Florent J, Godard C, Jung G, Lunel J, et al. Nosiheptide, a sulfur-  
520 containing peptide antibiotic isolated from *Streptomyces actuosus* 40037. *Experientia.*  
521 1980;36(4):414-6.
- 522 4. Procopio RE, Silva IR, Martins MK, Azevedo JL, Araujo JM. Antibiotics produced by  
523 *Streptomyces*. *Braz J Infect Dis.* 2012;16(5):466-71.
- 524 5. Nicolaou KC, Zak M, Rahimipour S, Estrada AA, Lee SH, O'Brate A, et al. Discovery of  
525 a biologically active thiostrepton fragment. *J Am Chem Soc.* 2005;127(43):15042-4.



- 526 6. Aminake MN, Schoof S, Sologub L, Leubner M, Kirschner M, Arndt HD, Pradel G.  
527 Thiostrepton and derivatives exhibit antimalarial and gametocytocidal activity by dually  
528 targeting parasite proteasome and apicoplast. *Antimicrob Agents Chemother.* 2011;55(4):1338-  
529 48.
- 530 7. Oman TJ, van der Donk WA. Follow the leader: the use of leader peptides to guide  
531 natural product biosynthesis. *Nat Chem Biol.* 2010;6(1):9-18.
- 532 8. Chekan JR, Ongpipattanakul C, Nair SK. Steric complementarity directs sequence  
533 promiscuous leader binding in RiPP biosynthesis. *Proc Natl Acad Sci U S A.*  
534 2019;116(48):24049-55.
- 535 9. Burkhart BJ, Kakkar N, Hudson GA, van der Donk WA, Mitchell DA. Chimeric Leader  
536 Peptides for the Generation of Non-Natural Hybrid RiPP Products. *ACS Cent Sci.*  
537 2017;3(6):629-38.
- 538 10. Burkhart BJ, Hudson GA, Dunbar KL, Mitchell DA. A prevalent peptide-binding domain  
539 guides ribosomal natural product biosynthesis. *Nat Chem Biol.* 2015;11(8):564-70.
- 540 11. Barr I, Latham JA, Iavarone AT, Chantarojsiri T, Hwang JD, Klinman JP. Demonstration  
541 That the Radical S-Adenosylmethionine (SAM) Enzyme PqqE Catalyzes de Novo Carbon-  
542 Carbon Cross-linking within a Peptide Substrate PqqA in the Presence of the Peptide Chaperone  
543 PqqD. *J Biol Chem.* 2016;291(17):8877-84.
- 544 12. Wieckowski BM, Hegemann JD, Mielcarek A, Boss L, Burghaus O, Marahiel MA. The  
545 PqqD homologous domain of the radical SAM enzyme ThnB is required for thioether bond  
546 formation during thurincin H maturation. *FEBS Lett.* 2015;589(15):1802-6.

- 547 13. Sumida T, Dubiley S, Wilcox B, Severinov K, Tagami S. Structural Basis of Leader  
548 Peptide Recognition in Lasso Peptide Biosynthesis Pathway. *ACS Chem Biol.* 2019;14(7):1619-  
549 27.
- 550 14. Grove TL, Himes PM, Hwang S, Yumerefendi H, Bonanno JB, Kuhlman B, et al.  
551 Structural Insights into Thioether Bond Formation in the Biosynthesis of Sactipeptides. *J Am*  
552 *Chem Soc.* 2017;139(34):11734-44.
- 553 15. Kretsch AM, Gadgil MG, DiCaprio AJ, Barrett SE, Kille BL, Si Y, et al. Peptidase  
554 Activation by a Leader Peptide-Bound RiPP Recognition Element. *Biochemistry.*  
555 2023;62(4):956-67.
- 556 16. Melby JO, Nard NJ, Mitchell DA. Thiazole/oxazole-modified microcins: complex natural  
557 products from ribosomal templates. *Curr Opin Chem Biol.* 2011;15(3):369-78.
- 558 17. Burkhart BJ, Schwalen CJ, Mann G, Naismith JH, Mitchell DA. YcaO-Dependent  
559 Posttranslational Amide Activation: Biosynthesis, Structure, and Function. *Chem Rev.*  
560 2017;117(8):5389-456.
- 561 18. Koehnke J, Bent AF, Zollman D, Smith K, Houssen WE, Zhu X, et al. The cyanobactin  
562 heterocyclase enzyme: a processive adenylase that operates with a defined order of reaction.  
563 *Angew Chem Int Ed Engl.* 2013;52(52):13991-6.
- 564 19. Koehnke J, Bent AF, Houssen WE, Mann G, Jaspars M, Naismith JH. The structural  
565 biology of patellamide biosynthesis. *Curr Opin Struct Biol.* 2014;29:112-21.
- 566 20. Koehnke J, Mann G, Bent AF, Ludewig H, Shirran S, Botting C, et al. Structural analysis  
567 of leader peptide binding enables leader-free cyanobactin processing. *Nat Chem Biol.*  
568 2015;11(8):558-63.

- 569 21. Dunbar KL, Melby JO, Mitchell DA. YcaO domains use ATP to activate amide  
570 backbones during peptide cyclodehydrations. *Nat Chem Biol.* 2012;8(6):569-75.
- 571 22. Ghilarov D, Stevenson CEM, Travin DY, Piskunova J, Serebryakova M, Maxwell A, et  
572 al. Architecture of Microcin B17 Synthetase: An Octameric Protein Complex Converting a  
573 Ribosomally Synthesized Peptide into a DNA Gyrase Poison. *Mol Cell.* 2019;73(4):749-62 e5.
- 574 23. Du Y, Qiu Y, Meng X, Feng J, Tao J, Liu W. A Heterotrimeric Dehydrogenase Complex  
575 Functions with 2 Distinct YcaO Proteins to Install 5 Azole Heterocycles into 35-Membered  
576 Sulfomycin Thiopeptides. *J Am Chem Soc.* 2020;142(18):8454-63.
- 577 24. McIntosh JA, Donia MS, Schmidt EW. Insights into heterocyclization from two highly  
578 similar enzymes. *J Am Chem Soc.* 2010;132(12):4089-91.
- 579 25. McIntosh JA, Schmidt EW. Marine molecular machines: heterocyclization in  
580 cyanobactin biosynthesis. *Chembiochem.* 2010;11(10):1413-21.
- 581 26. Dunbar KL, Tietz JI, Cox CL, Burkhardt BJ, Mitchell DA. Identification of an Auxiliary  
582 Leader Peptide-Binding Protein Required for Azoline Formation in Ribosomal Natural Products.  
583 *J Am Chem Soc.* 2015;137(24):7672-7.
- 584 27. Melby JO, Dunbar KL, Trinh NQ, Mitchell DA. Selectivity, directionality, and  
585 promiscuity in peptide processing from a *Bacillus* sp. Al Hakam cyclodehydratase. *J Am Chem*  
586 *Soc.* 2012;134(11):5309-16.
- 587 28. Regni CA, Roush RF, Miller DJ, Nourse A, Walsh CT, Schulman BA. How the MccB  
588 bacterial ancestor of ubiquitin E1 initiates biosynthesis of the microcin C7 antibiotic. *EMBO J.*  
589 2009;28(13):1953-64.

- 590 29. Egawa Y, Umino K, Tamura Y, Shimizu M, Kaneko K. Sulfomycins, a series of new  
591 sulfur-containing antibiotics. I. Isolation, purification and properties. *J Antibiot (Tokyo)*.  
592 1969;22(1):12-7.
- 593 30. Bennallack PR, Burt SR, Heder MJ, Robison RA, Griffiths JS. Characterization of a novel  
594 plasmid-borne thiopeptide gene cluster in *Staphylococcus epidermidis* strain 115. *J Bacteriol*.  
595 2014;196(24):4344-50.
- 596 31. Bennallack PR, Bewley KD, Burlingame MA, Robison RA, Miller SM, Griffiths JS.  
597 Reconstitution and Minimization of a Micrococcin Biosynthetic Pathway in *Bacillus subtilis*. *J*  
598 *Bacteriol*. 2016;198(18):2431-8.
- 599 32. Bennallack PR, Griffiths JS. Elucidating and engineering thiopeptide biosynthesis. *World*  
600 *J Microbiol Biotechnol*. 2017;33(6):119.
- 601 33. Bewley KD, Bennallack PR, Burlingame MA, Robison RA, Griffiths JS, Miller SM.  
602 Capture of micrococcin biosynthetic intermediates reveals C-terminal processing as an  
603 obligatory step for in vivo maturation. *Proc Natl Acad Sci U S A*. 2016;113(44):12450-5.
- 604 34. Liao R, Duan L, Lei C, Pan H, Ding Y, Zhang Q, et al. Thiopeptide biosynthesis  
605 featuring ribosomally synthesized precursor peptides and conserved posttranslational  
606 modifications. *Chem Biol*. 2009;16(2):141-7.
- 607 35. Wieland Brown LC, Acker MG, Clardy J, Walsh CT, Fischbach MA. Thirteen  
608 posttranslational modifications convert a 14-residue peptide into the antibiotic thiocillin. *Proc*  
609 *Natl Acad Sci U S A*. 2009;106(8):2549-53.
- 610 36. Soding J, Biegert A, Lupas AN. The HHpred interactive server for protein homology  
611 detection and structure prediction. *Nucleic Acids Res*. 2005;33(Web Server issue):W244-8.

- 612 37. Zimmermann L, Stephens A, Nam SZ, Rau D, Kubler J, Lozajic M, et al. A Completely  
613 Reimplemented MPI Bioinformatics Toolkit with a New HHpred Server at its Core. *J Mol Biol.*  
614 2018;430(15):2237-43.
- 615 38. Gabler F, Nam SZ, Till S, Mirdita M, Steinegger M, Soding J, et al. Protein Sequence  
616 Analysis Using the MPI Bioinformatics Toolkit. *Curr Protoc Bioinformatics.* 2020;72(1):e108.
- 617 39. Mitchell DA, Lee SW, Pence MA, Markley AL, Limm JD, Nizet V, Dixon JE. Structural  
618 and functional dissection of the heterocyclic peptide cytotoxin streptolysin S. *J Biol Chem.*  
619 2009;284(19):13004-12.
- 620 40. Roy RS, Kim S, Baleja JD, Walsh CT. Role of the microcin B17 propeptide in substrate  
621 recognition: solution structure and mutational analysis of McbA1-26. *Chem Biol.* 1998;5(4):217-  
622 28.
- 623 41. Melby JO, Li X, Mitchell DA. Orchestration of enzymatic processing by  
624 thiazole/oxazole-modified microcin dehydrogenases. *Biochemistry.* 2014;53(2):413-22.
- 625 42. Dunbar KL, Chekan JR, Cox CL, Burkhart BJ, Nair SK, Mitchell DA. Discovery of a  
626 new ATP-binding motif involved in peptidic azoline biosynthesis. *Nat Chem Biol.*  
627 2014;10(10):823-9.
- 628 43. Khusainov R, Kuipers OP. When the leader gets loose: in vivo biosynthesis of a  
629 leaderless prenisin is stimulated by a trans-acting leader peptide. *Chembiochem.*  
630 2012;13(16):2433-8.
- 631 44. Oman TJ, Knerr PJ, Bindman NA, Velasquez JE, van der Donk WA. An engineered  
632 lantibiotic synthetase that does not require a leader peptide on its substrate. *J Am Chem Soc.*  
633 2012;134(16):6952-5.

- 634 45. Thibodeaux CJ, Wagoner J, Yu Y, van der Donk WA. Leader Peptide Establishes  
635 Dehydration Order, Promotes Efficiency, and Ensures Fidelity During Lactacin 481 Biosynthesis.  
636 J Am Chem Soc. 2016;138(20):6436-44.
- 637 46. Goto Y, Ito Y, Kato Y, Tsunoda S, Suga H. One-pot synthesis of azoline-containing  
638 peptides in a cell-free translation system integrated with a posttranslational cyclodehydratase.  
639 Chem Biol. 2014;21(6):766-74.
- 640 47. Dunbar KL, Mitchell DA. Insights into the mechanism of peptide cyclodehydrations  
641 achieved through the chemoenzymatic generation of amide derivatives. J Am Chem Soc.  
642 2013;135(23):8692-701.
- 643 48. Mavaro A, Abts A, Bakkes PJ, Moll GN, Driessen AJM, Smits SHJ, Schmitt L. Substrate  
644 recognition and specificity of the NisB protein, the lantibiotic dehydratase involved in nisin  
645 biosynthesis. J Biol Chem. 2011;286(35):30552-60.
- 646 49. Ortega MA, Hao Y, Zhang Q, Walker MC, van der Donk WA, Nair SK. Structure and  
647 mechanism of the tRNA-dependent lantibiotic dehydratase NisB. Nature. 2015;517(7535):509-  
648 12.
- 649 50. Schmidt EW, Nelson JT, Rasko DA, Sudek S, Eisen JA, Haygood MG, Ravel J.  
650 Patellamide A and C biosynthesis by a microcin-like pathway in *Prochloron didemni*, the  
651 cyanobacterial symbiont of *Lissoclinum patella*. Proc Natl Acad Sci U S A. 2005;102(20):7315-  
652 20.
- 653 51. Jumper J, Evans R, Pritzel A, Green T, Figurnov M, Ronneberger O, et al. Highly  
654 accurate protein structure prediction with AlphaFold. Nature. 2021;596(7873):583-9.
- 655 52. Mirdita M, Schutze K, Moriwaki Y, Heo L, Ovchinnikov S, Steinegger M. ColabFold:  
656 making protein folding accessible to all. Nat Methods. 2022;19(6):679-82.

- 657 53. Tyka MD, Keedy DA, Andre I, Dimaio F, Song Y, Richardson DC, et al. Alternate states  
658 of proteins revealed by detailed energy landscape mapping. *J Mol Biol.* 2011;405(2):607-18.
- 659 54. Park H, Bradley P, Greisen P, Jr., Liu Y, Mulligan VK, Kim DE, et al. Simultaneous  
660 Optimization of Biomolecular Energy Functions on Features from Small Molecules and  
661 Macromolecules. *J Chem Theory Comput.* 2016;12(12):6201-12.
- 662 55. Alford RF, Leaver-Fay A, Jeliazkov JR, O'Meara MJ, DiMaio FP, Park H, et al. The  
663 Rosetta All-Atom Energy Function for Macromolecular Modeling and Design. *J Chem Theory*  
664 *Comput.* 2017;13(6):3031-48.
- 665 56. Lawrence MC, Colman PM. Shape complementarity at protein/protein interfaces. *J Mol*  
666 *Biol.* 1993;234(4):946-50.
- 667 57. Benjamini Y, Krieger AM, Yekutieli D. Adaptive linear step-up procedures that control  
668 the false discovery rate. *Biometrika.* 2006;93(3):491-507.

669

670

671

672

673

## 674 FIGURE LEGENDS

675 **Figure 1. Schematic models of TOMM complexes from four RiPP biosynthetic pathways**  
676 **for which the structural architecture has been elucidated.** Color codes for each protein are  
677 described on the box on the right. The cyclodehydratase enzyme from the YcaO superfamily is  
678 labeled YcaO. Black lines represent fused proteins, and dotted rectangles denote non-covalent  
679 interactions. A. Cartoon representation of the cyclodehydratase form the Trunkamide

680 biosynthetic pathway (PDB: 4BS9) (18). B. Interactions between TOMM proteins from the  
681 microcin Heterocycloanthracin. The question mark denotes that the dehydrogenase is part of this  
682 pathway but attempts to characterize their protein interactions have not been successful (26). C.  
683 Cartoon diagram based on the crystal structure of Microcin B17 (PDB: 6GRI) (22) D. Paradigm  
684 of interactions between TOMM proteins in the biosynthesis of the thiopeptide sulfomycin.  
685 Heterocycle formation in this system is mediated by three complexes labeled 1, 2, and 3 (23).

686

687 **Figure 2. Genes and proteins controlling micrococcin biosynthesis.** A. Map of the native *tcl*  
688 gene cluster from *M. caseolyticus*. Essential proteins for complete micrococcin production are  
689 annotated by colored blocks at the bottom. The gene encoding the precursor peptide (TclE) is  
690 colored black, and the genes encoding proteins for thiazole installation (TclI, TclJ, TclN) are  
691 colored blue. B. Overview of the micrococcin biosynthetic pathway that converts the TclE core  
692 peptide into micrococcin. Modifications and corresponding enzymes are color coded.  
693 Abbreviations: Tz, thiazolyl; Dc, decarboxyl; Dh, dehydro. C. Two-step conversion of TclE Cys  
694 residues to thiazole by the enzymes TclJ, and TclN.

695

696 **Figure 3. Characterization of functional expression of Tcl TOMM proteins from *E. coli*.**  
697 MS analysis (MALDI-TOF) of thiazole installation on TclE using purified components from *E.*  
698 *coli*. Reactions included TEV protease to cleave the leader-core region of TclE from the GST tag  
699 prior to mass spectrometry analysis. Numbers 1-4 on the left side of each MALDI-TOF spectra  
700 represent each of the four strains we used to express the Tcl proteins.

701



702 **Figure 4. RRE of TcII interacts with TcIE.** A. AlphaFold2 model of the TcIE:TcII dimer. TcIE  
703 is shown in yellow. TcII<sub>NTD</sub> is highlighted in red, while TcII<sub>CTD</sub> is shown in brown. Residues  
704 featuring key protein interactions are labeled as follows: TcII<sub>NTD</sub> (residues F7, V30, V31, I74,  
705 V74, K78, N27, K22) in red, and TcIE (residues F17, E21, E22, E28) in yellow. B. SDS-PAGE  
706 analysis with coomassie blue staining to detect TcIE:TcII<sub>NTD</sub> interactions. Protein identities are  
707 given on the right side of the gel, and information of samples loaded in each lane is given above  
708 the gel.

709  
710 **Figure 5. TcIE leader truncation analysis.** A. Schematic diagram of TcIE leader truncations.  
711 Native TcIE from *M. caseolyticus* is shown on top followed by the mutagenesis analysis on the  
712 N-terminus of the TcIE leader. B. Nickel copurification experiment to detect TcII<sub>NTD</sub> interactions  
713 with truncated variants of the TcIE leader. The top panel shows the TcI proteins that were co-  
714 expressed for this experiment. His-tagged TcII<sub>NTD</sub> was co-expressed with each TcIE leader  
715 truncated variant in *E. coli* and subjected to purification with nickel-NTA beads and SDS-PAGE.  
716 Protein identities are given on the right side of the gel. For each GST-TcIE truncation variant, the  
717 molecular weights are as follows: Δ3 (31.4 kDa), Δ6 (31.0 kDa), Δ9 (30.7 kDa), Δ12 (30.4 kDa),  
718 Δ15 (30.1 kDa), Δ18 (29.7 kDa).

719  
720 **Figure 6. Effects of TcIE leader truncations on the production of fully modified core**  
721 **peptides.** Fully modified TcIE is defined by the presence of six thiazoles in the core peptide.  
722 Each bar shows percentage of TcIE peptides detected by LC-MS that are fully modified. Each  
723 TcIE truncated variant (see Fig. 4A; Δ9, Δ12, Δ15, and Δ18) was co-expressed with TcII, TcIJ,  
724 and TcIN in *E. coli* and purified for LC-MS. Reactions included TEV protease to cleave TcIE

725 from the GST tag prior to LC-MS analysis. Data are shown as the mean of three independent  
726 replicates with standard deviation. Asterisks show statically significant differences ( $P < 0.05$ )  
727 according to a parametric t-test carried out with the Benjamini, Krieger, and Yekutieli method  
728 (57).

729

730 **Figure 7. Domain analysis of TcII binding to TcIJ and TcIN.** SDS-PAGE analysis to detect  
731 TcI protein expression and copurification. Maps of His-tagged TcII, TcII<sub>CTD</sub>, TcIJ and TcIN used  
732 in this study are shown above the gel. Asterisk shows a weak band corresponding to TcIN that  
733 does not appear in the vector only control (Lane 1) but consistently appears in independently  
734 replicated gels. The weak nature of this band could be explained by TcIN being degraded by  
735 proteases or weak interactions with TcII<sub>NTD</sub>.

736

737 **Figure 8. Analysis of TcII, TcIJ and TcIN interactions as a stable complex.** Coomassie-  
738 stained SDS-PAGE of purified TcIIJN proteins expressed together in *E. coli* to detect complex  
739 formation. The upper panel shows the combinations of each his-tagged TcI protein. The  
740 difference between Lane 5 and Lane 7 is that, in Lane 7, the linker between TcIJ and the histidine  
741 tag is longer (6-Gly) compared to the normal linker (Gly-Gly-Ser) used in Lane 5 and in the  
742 other Lanes. Asterisks denote weak protein bands that do not appear in the vector only control  
743 (Lane 1) but consistently show up in replicated copurification experiments.

744 **Figure 9. Predicted AlphaFold2 models of the TcII:TcIJ (A) and TcII:TcIN (B) dimers.**  
745 TcII<sub>NTD</sub> is shown in red, and TcII<sub>CTD</sub> is shown in brown with the central Helix 6 highlighted in  
746 magenta. TcIJ is depicted in cyan and TcIN is shown in green.

747

748 **Figure 10. Dissection of Helix 6 on TcII to determine key interactions with TcIJ and TcIN.**

749 A. Nickel copurification experiment with His-tagged TcII with its corresponding Helix 6  
750 substitution co-expressed with TcIJ and TcIN. Each substitution on TcII is labeled on each lane.

751 B. Depiction of Helix 6 highlighting key residues for interacting with TcIJ in cyan (Y189, I198,  
752 I202, T212) and TcIN in green (H194, N201, S205, F208, L209). Residues highlighted in gray  
753 (T188, L197, C199, E206, Y210, S213) had no effect in TcII interactions with either TcIJ or  
754 TcIN (see Fig. S2).

755

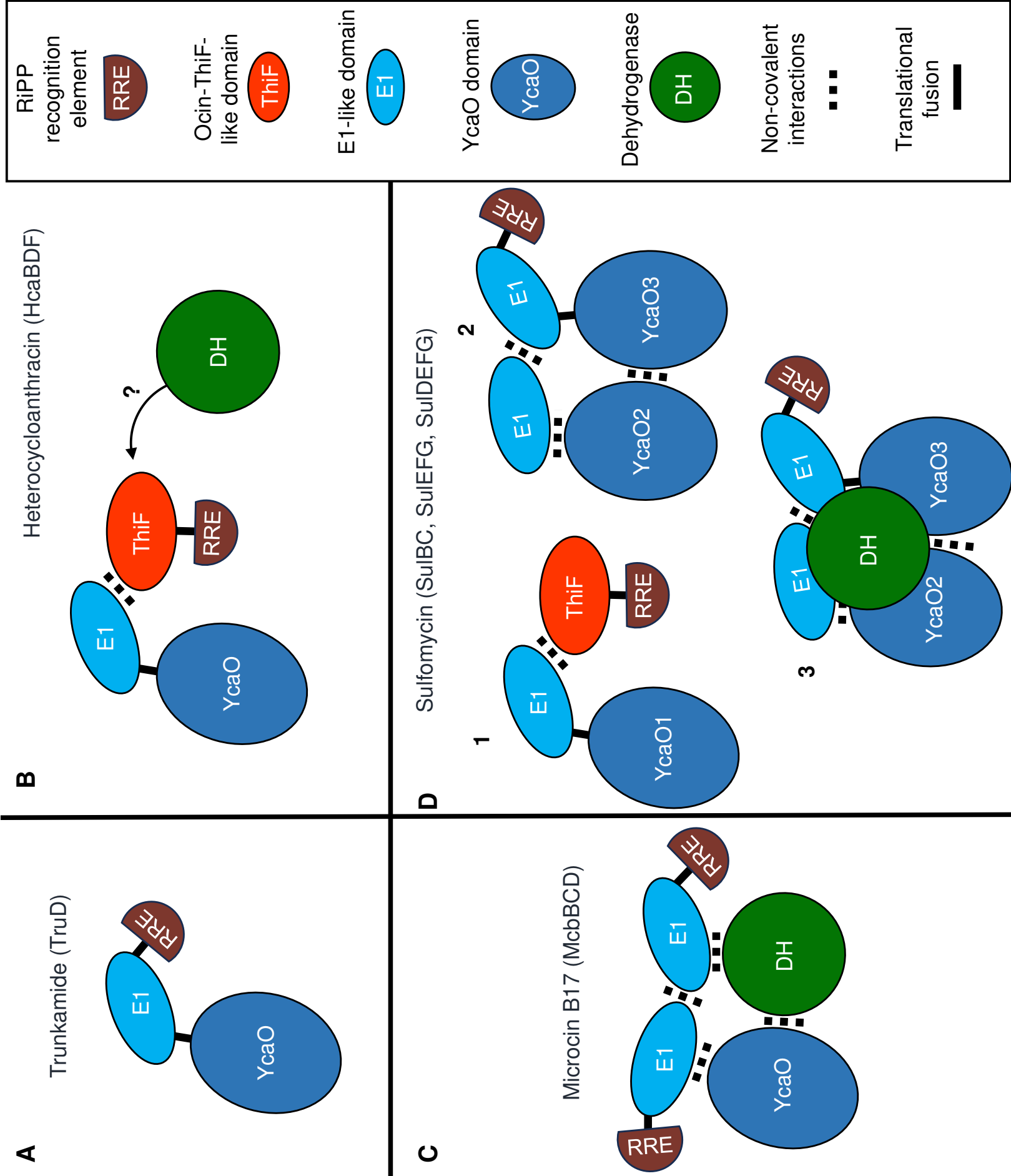
756 **Figure 11. E1-like domain analysis of TcIJ.** A. Map of TcIJ highlighting its E1-like and YcaO  
757 domains. Labeled are the two NTD fragments of TcIJ used in this study. B. SDS-PAGE analysis  
758 to detect interactions between the two TcIJ<sub>NTD</sub> fragments (NTD1, and NTD2) and TcII.

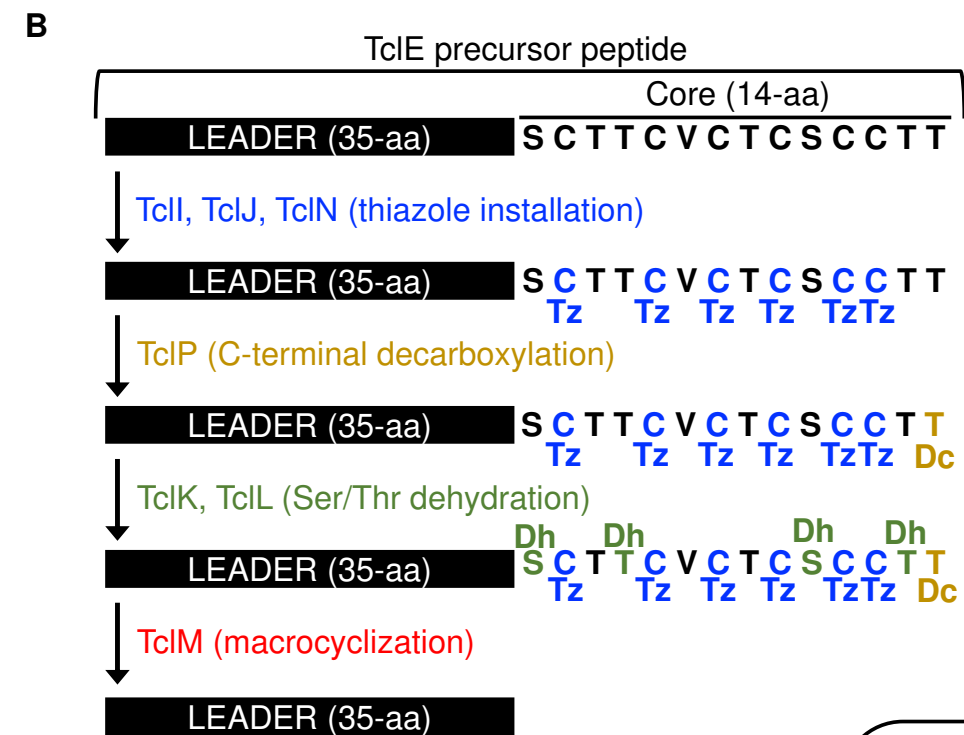
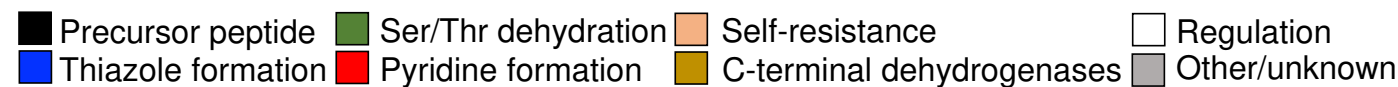
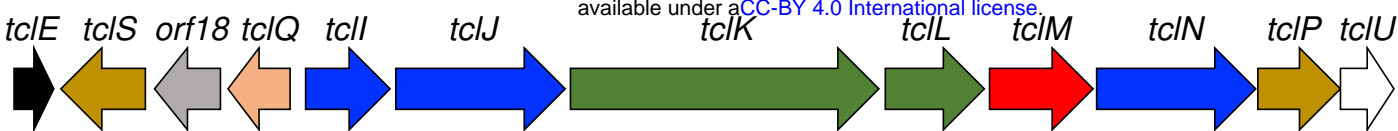
759

760 **Figure 12. Size-exclusion chromatography of purified TcII and TcIIN.** Yellow dotted line  
761 indicates chromatogram of purified TcII. Grey dotted line shows the chromatograph for the  
762 TcIIN purified complex. The blue chromatogram represents the protein ladder, and the dotted  
763 orange line shows the chromatogram for the buffer only control.

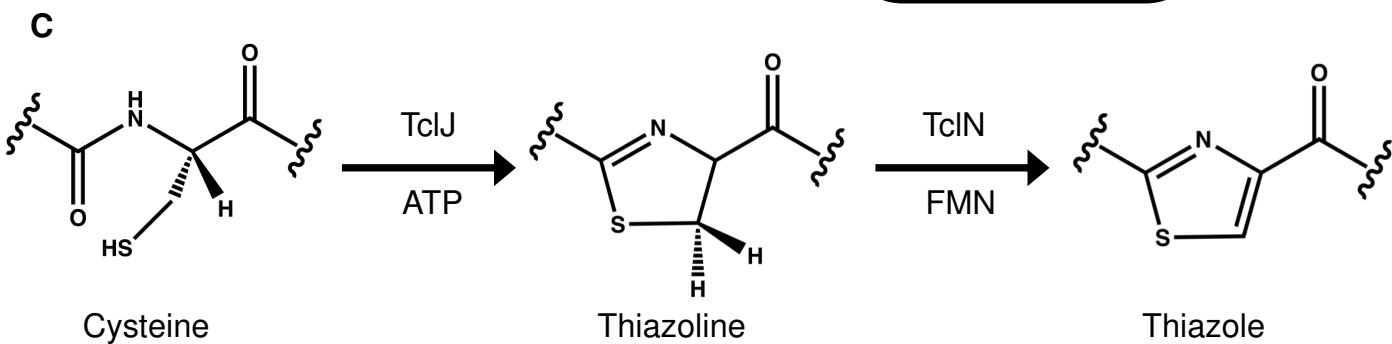
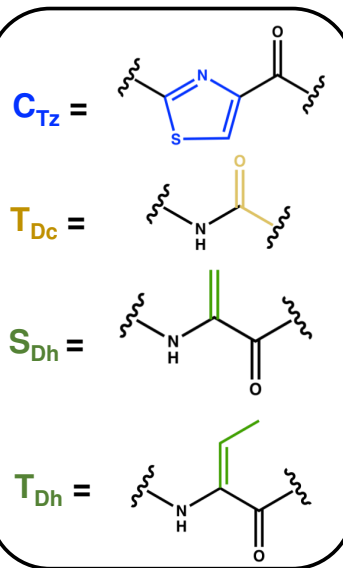
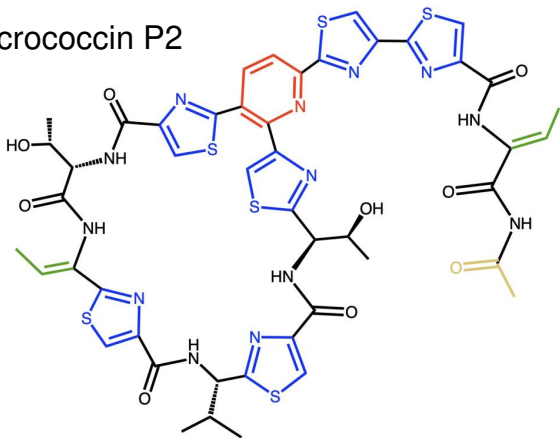
764

765 **Figure 13. Paradigm for cysteine to thiazole conversion by TcII, TcIJ and TcIN on the**  
766 **precursor peptide TcIE in the biosynthesis of micrococcin.** Schematic model of the two  
767 functional complexes (TcII:TcIJ, and TcII:TcIN) that assemble to achieve two-step thiazole  
768 installation on the core of TcIE.



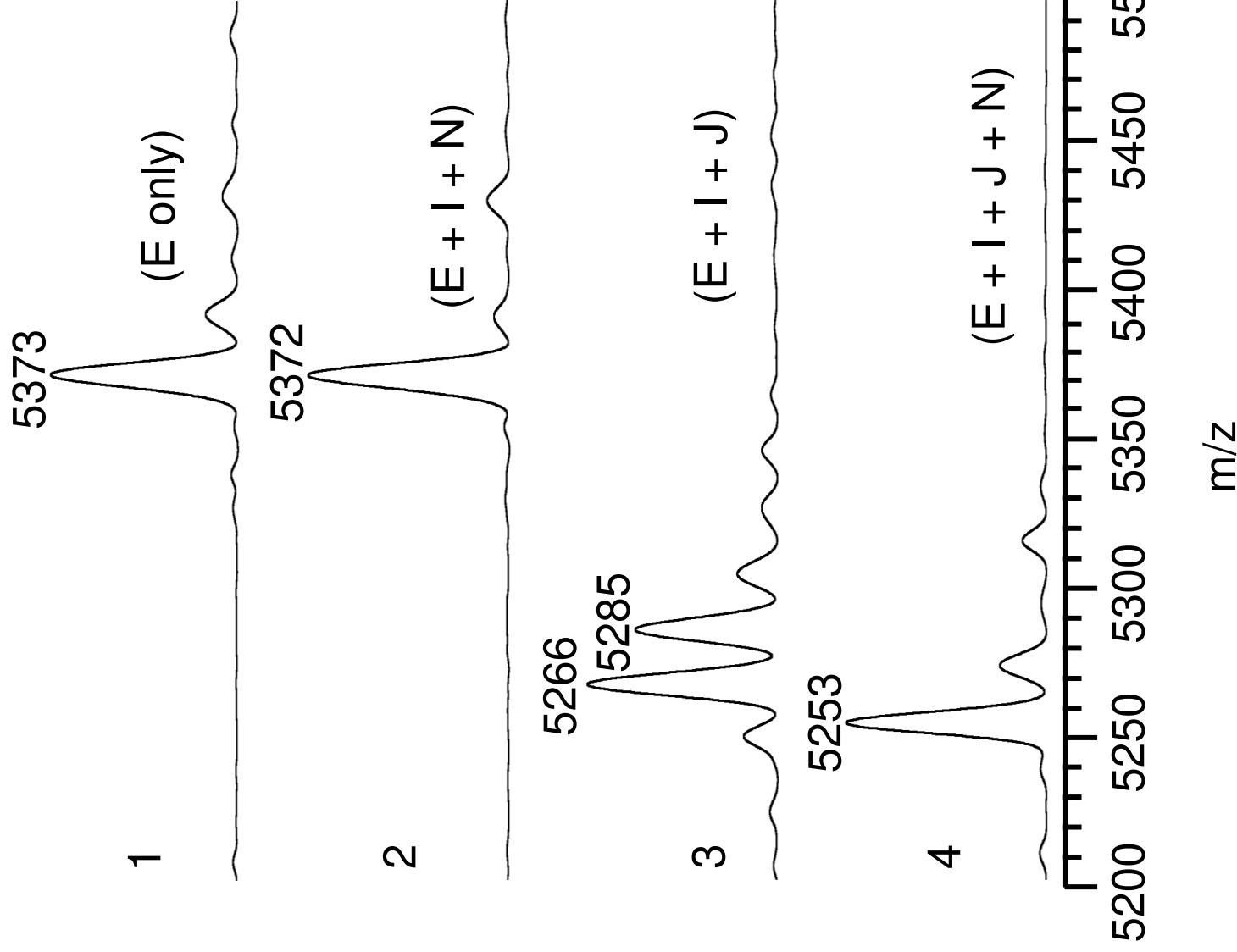


+  
Micrococcin P2

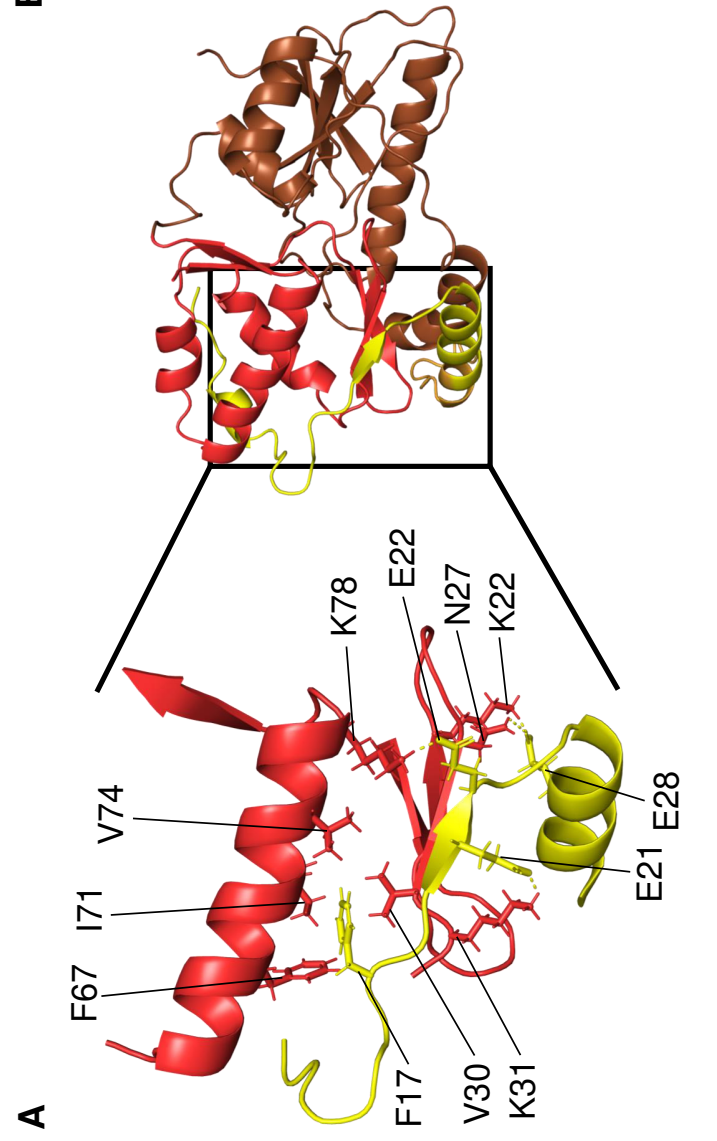


Strains

	1	2	3	4
GST-TcIE	+	+	+	+
TcII + TcIN	-	+	-	-
TcII + TcIJ	-	-	+	-
TcII + TcIJ + TcIN	-	-	-	+



TcIE peptide species	Calculated mass [M+H] <sup>+</sup>
unmodified	5373.9
6 x thiazole	5253.7
6 x thiazoline	5265.8
5 x thiazoline	5283.8

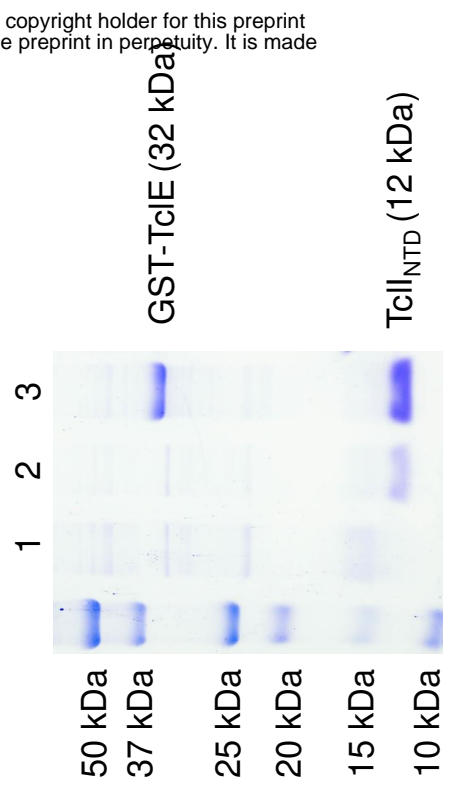


**B** Lane 1: Vector only control

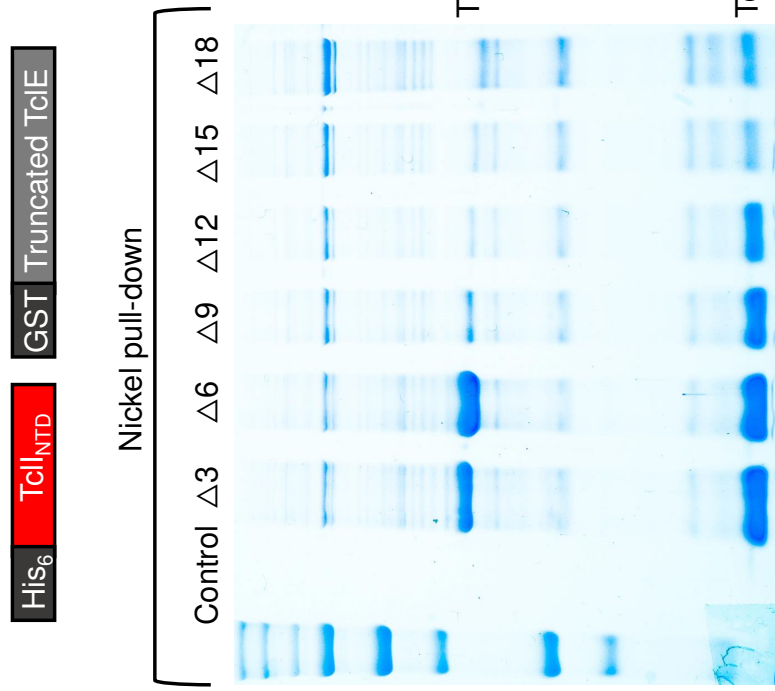
Lane 2: His<sub>6</sub> TcII<sub>NTD</sub>

Lane 3: His<sub>6</sub> TcII<sub>NTD</sub>

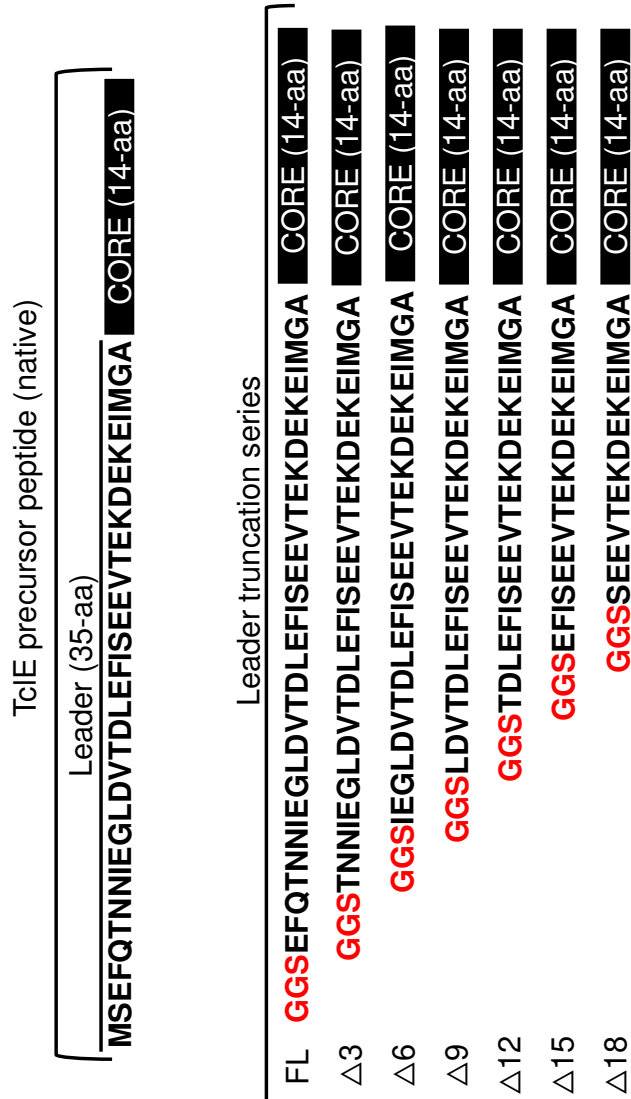
GST TcIE



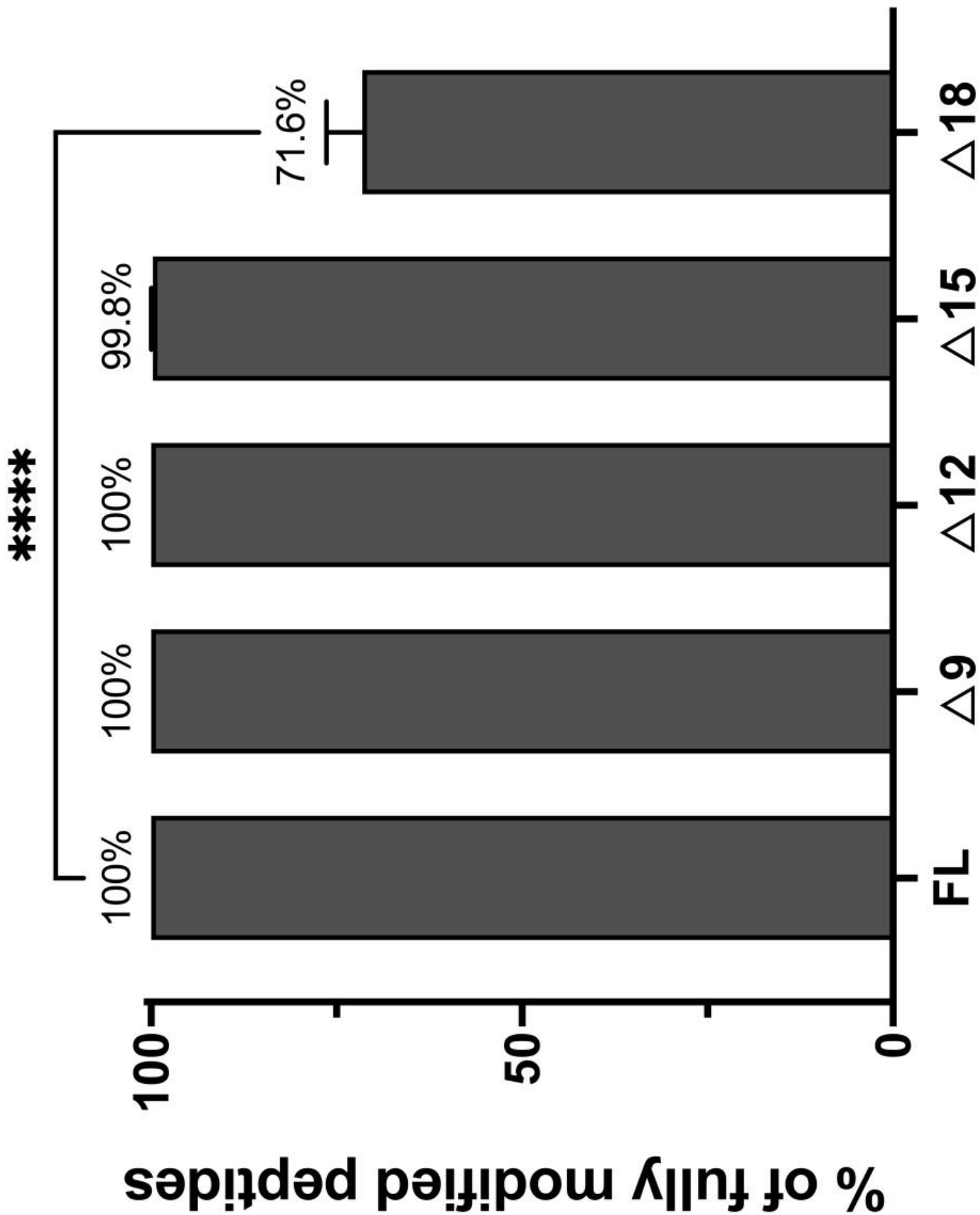
**B**

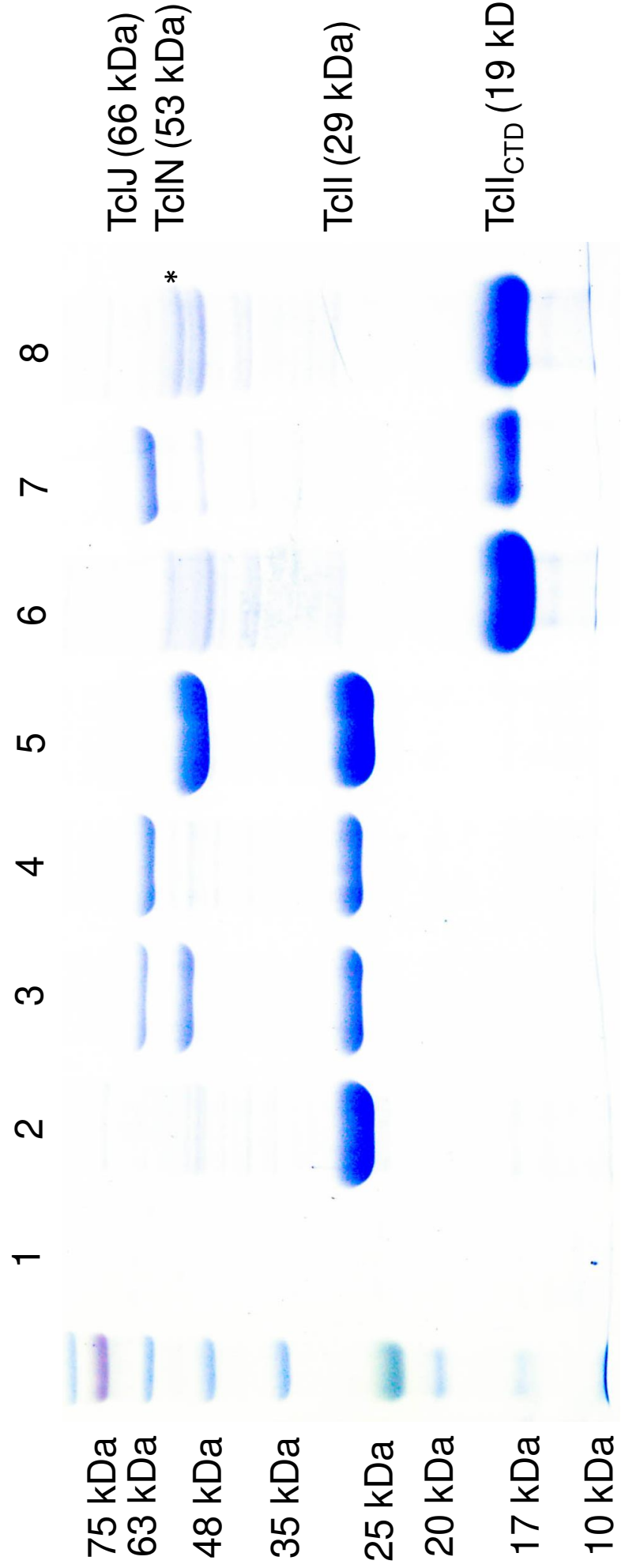
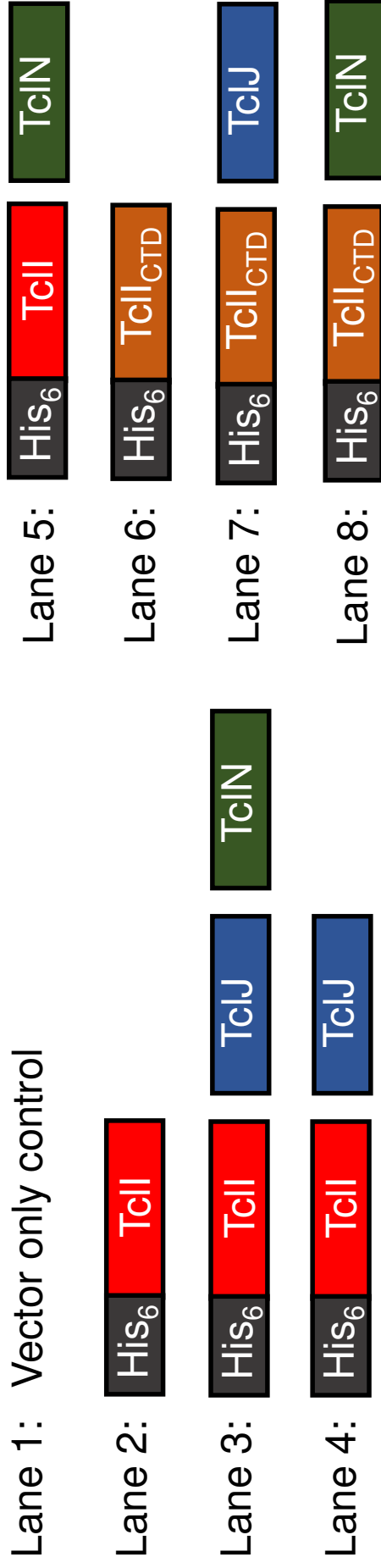


**A**

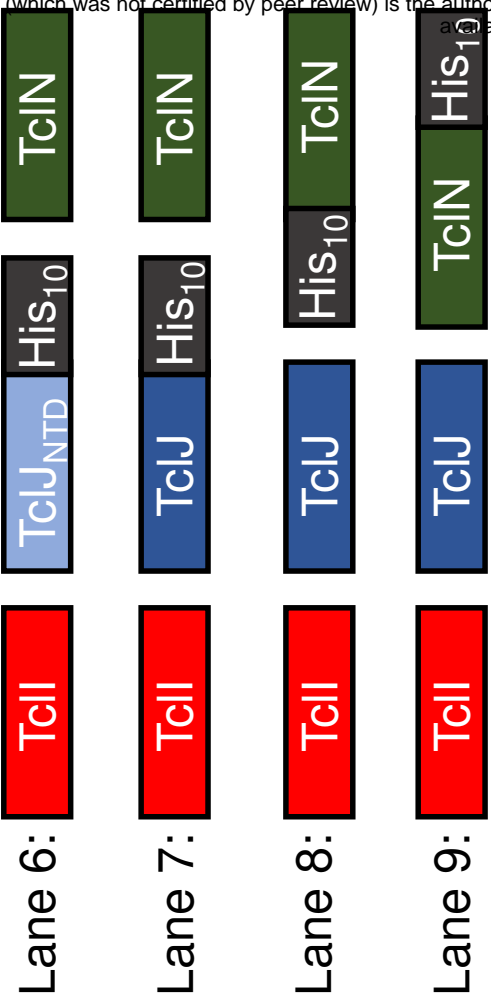
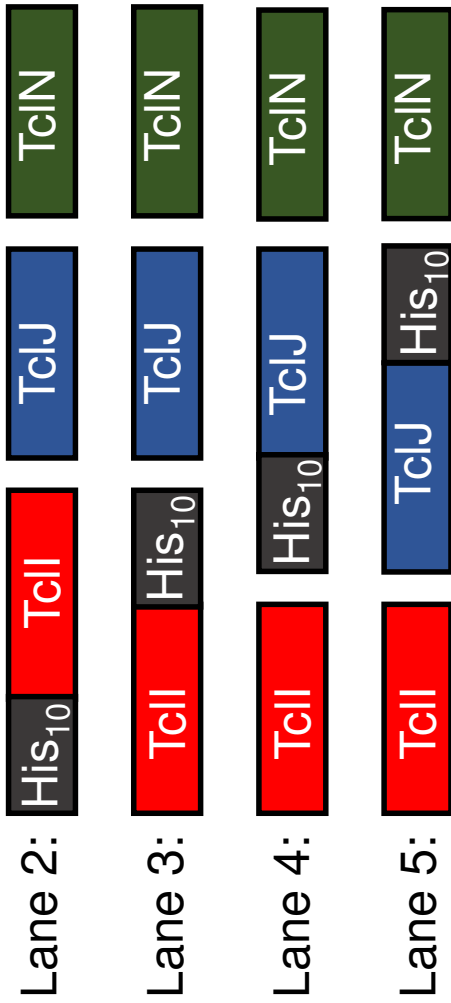




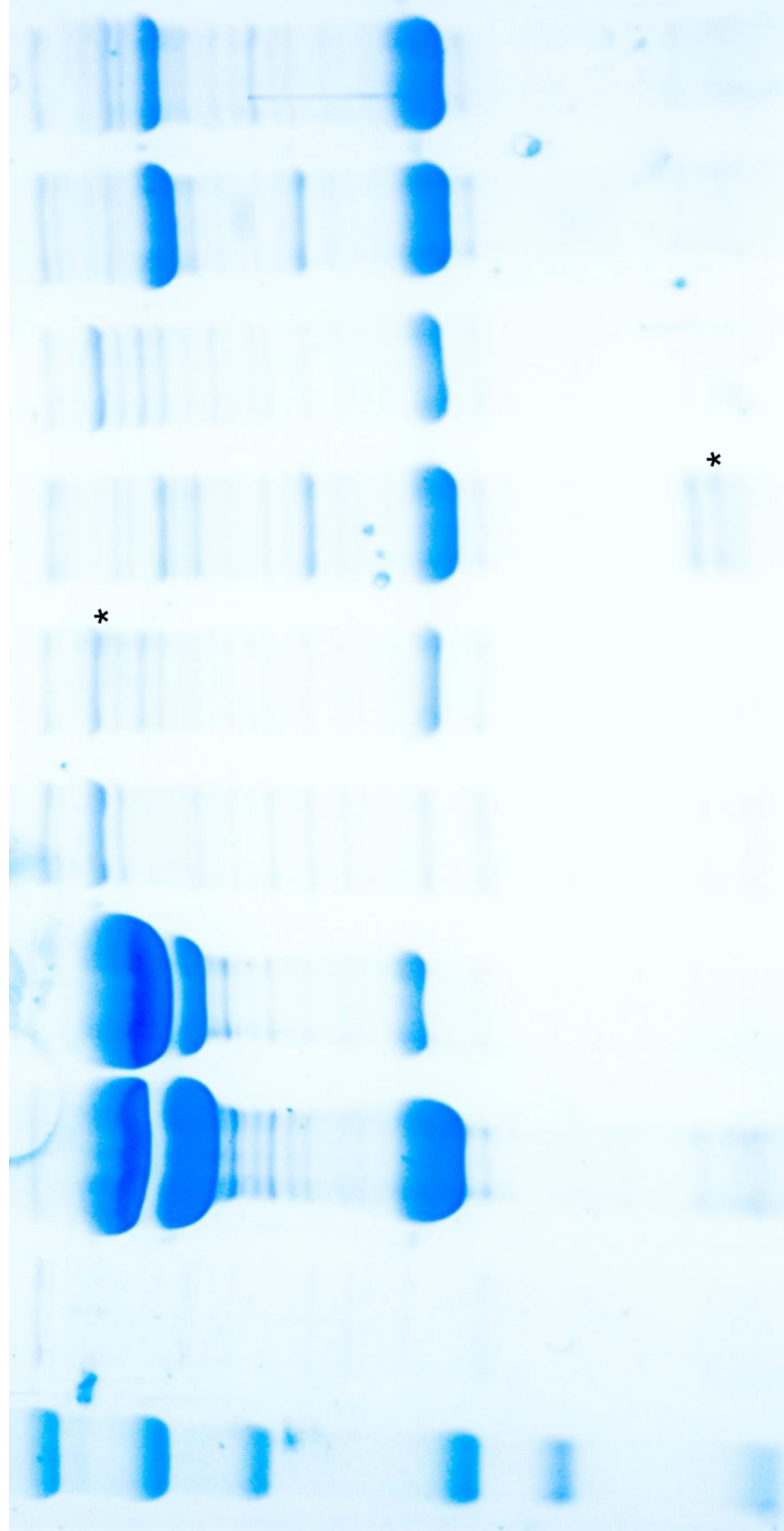




Lane 1: Vector only control



1 2 3 4 5 6 7 8 9



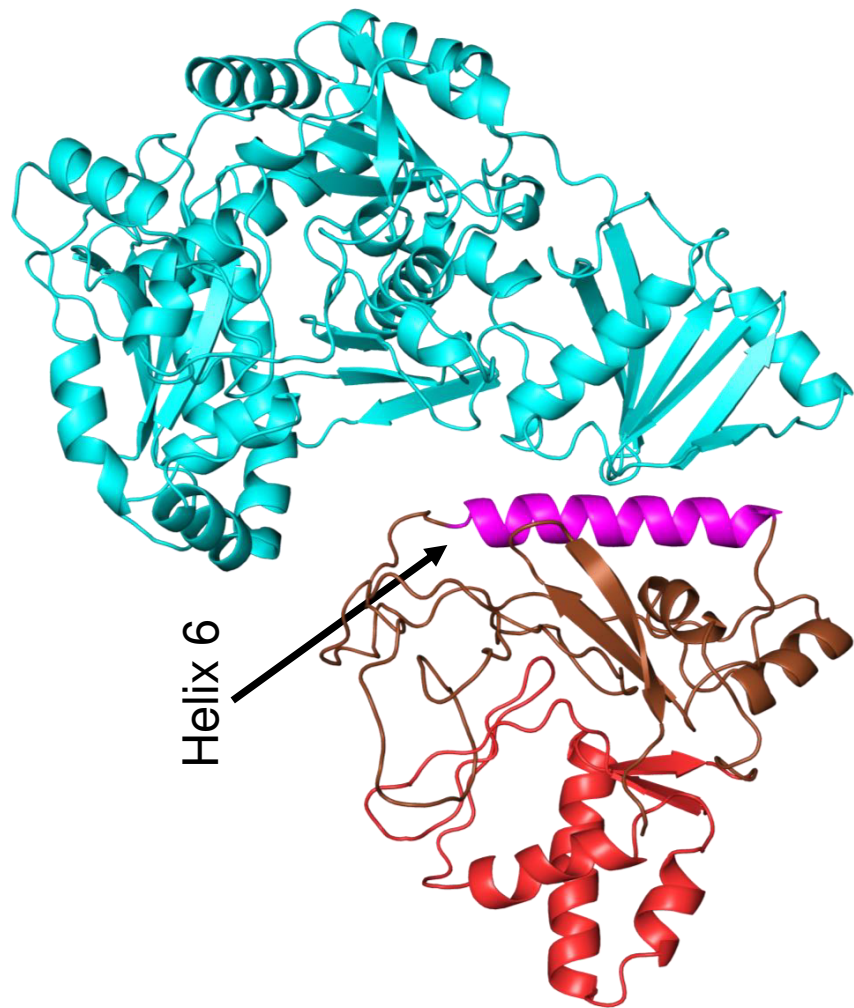
TcIJ (66 kDa)  
TcIN (53 kDa)

TcII (29 kDa)

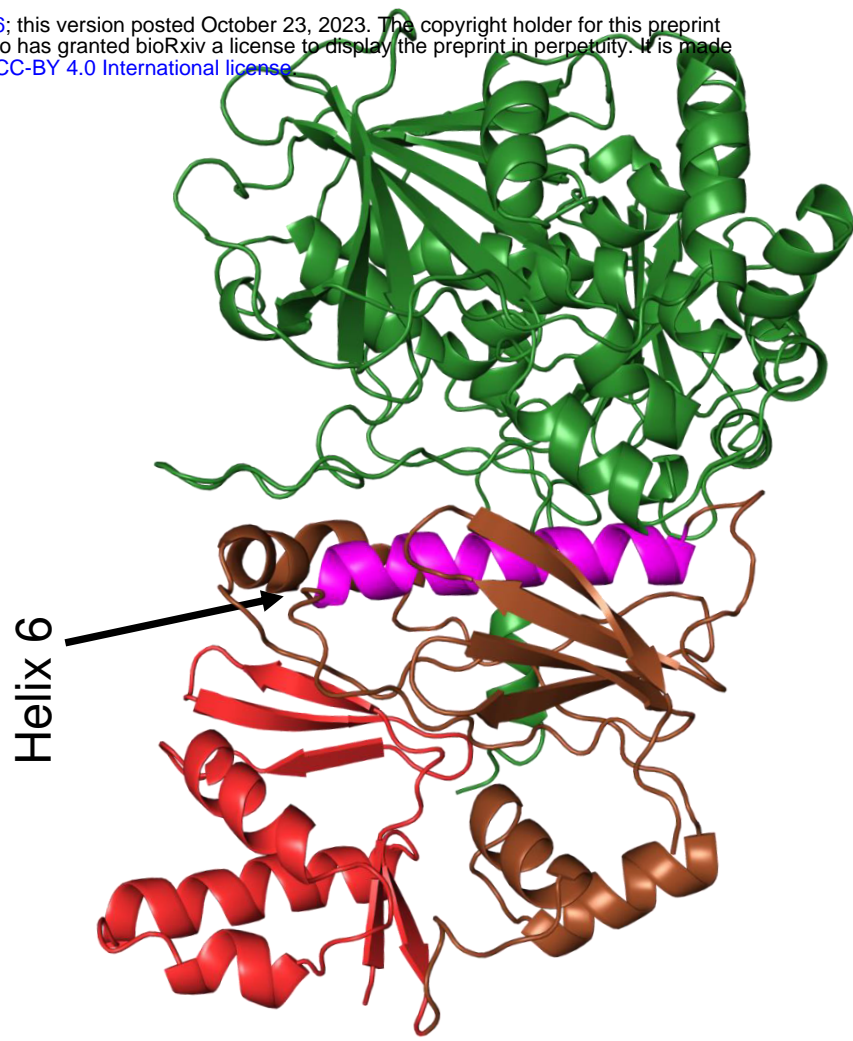
TcIJ<sub>NTD</sub> (15 kDa)

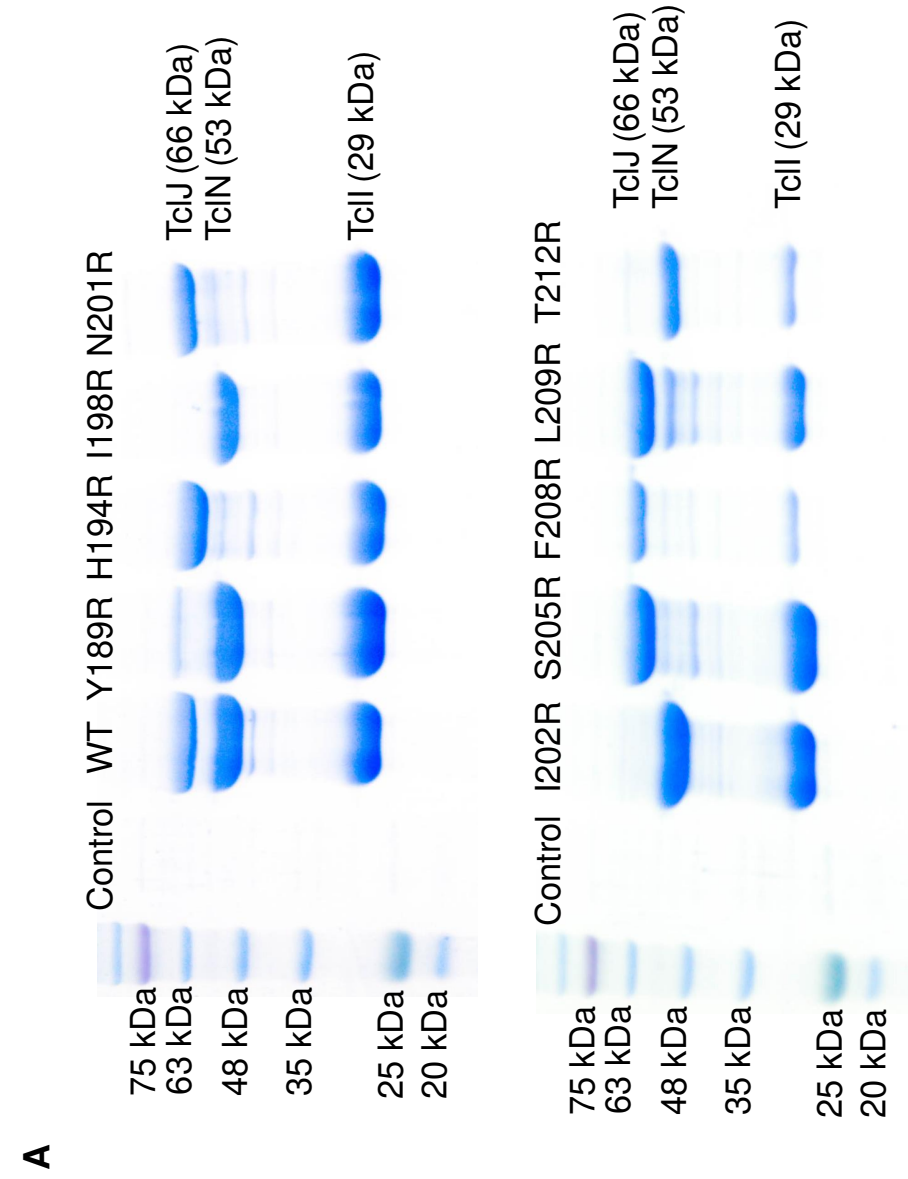
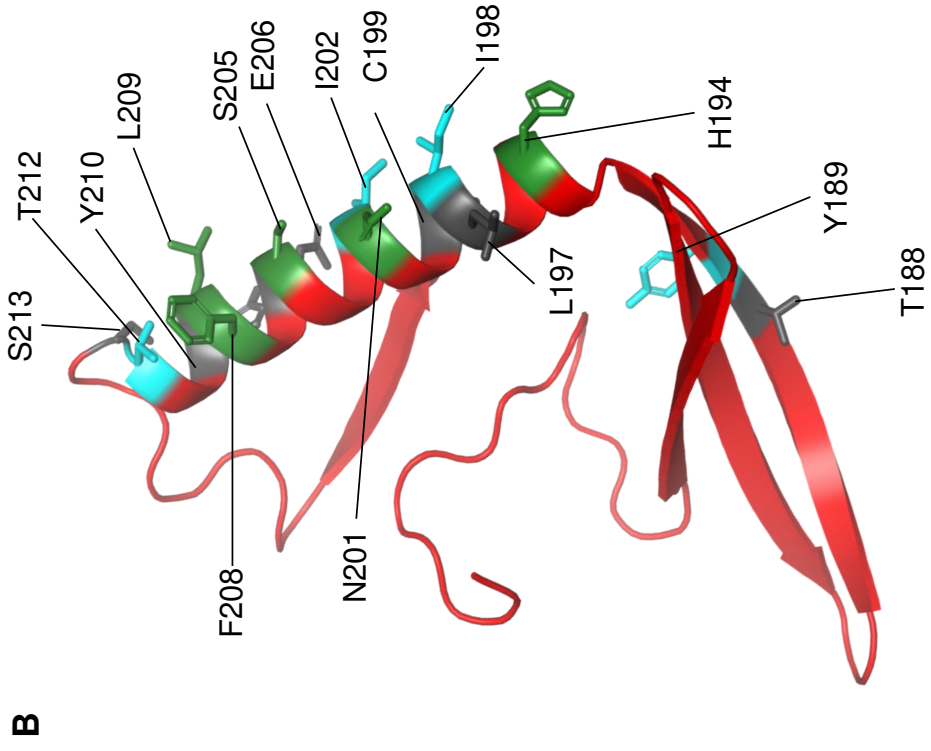
75 kDa  
50 kDa  
37 kDa  
25 kDa  
20 kDa  
15 kDa

**A**

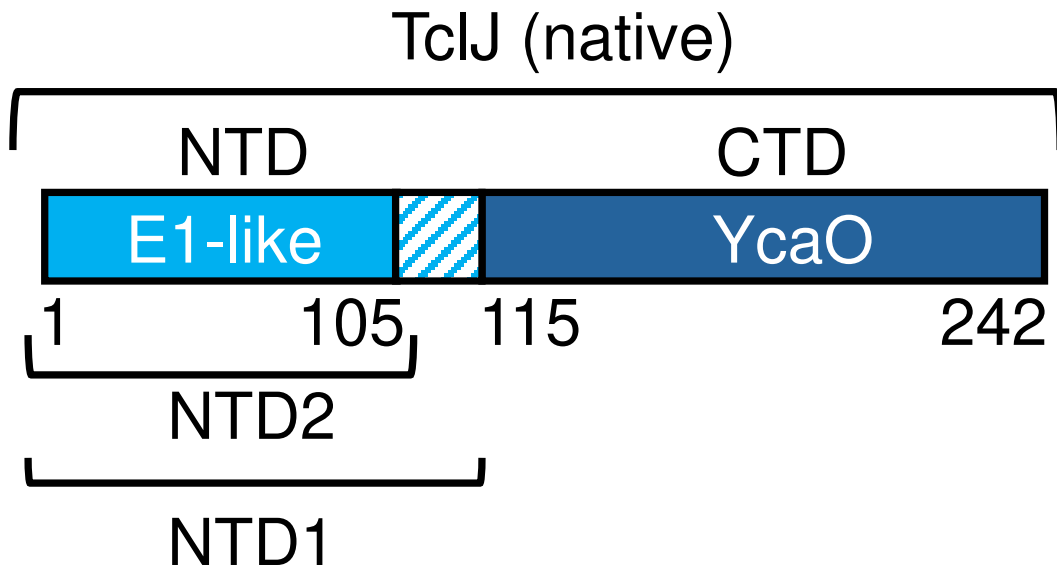


**B**





**A**



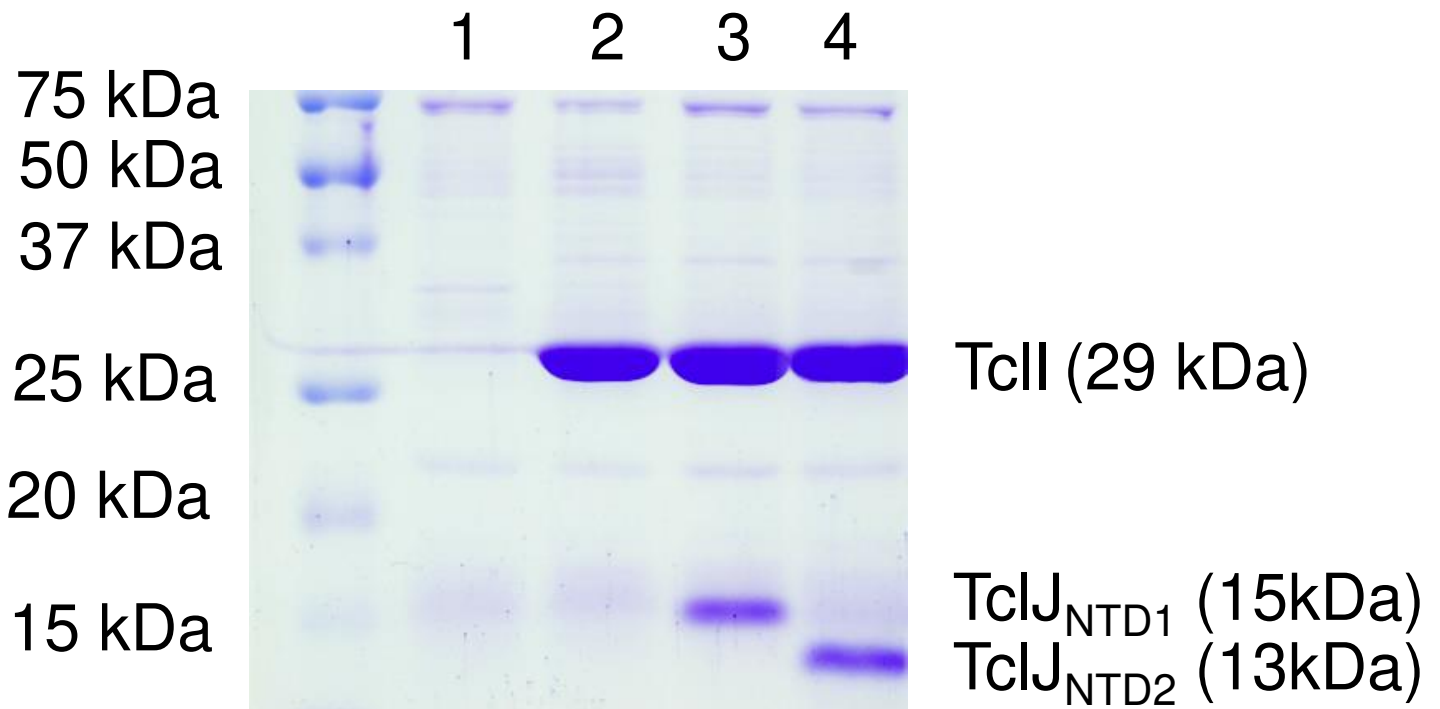
**B**

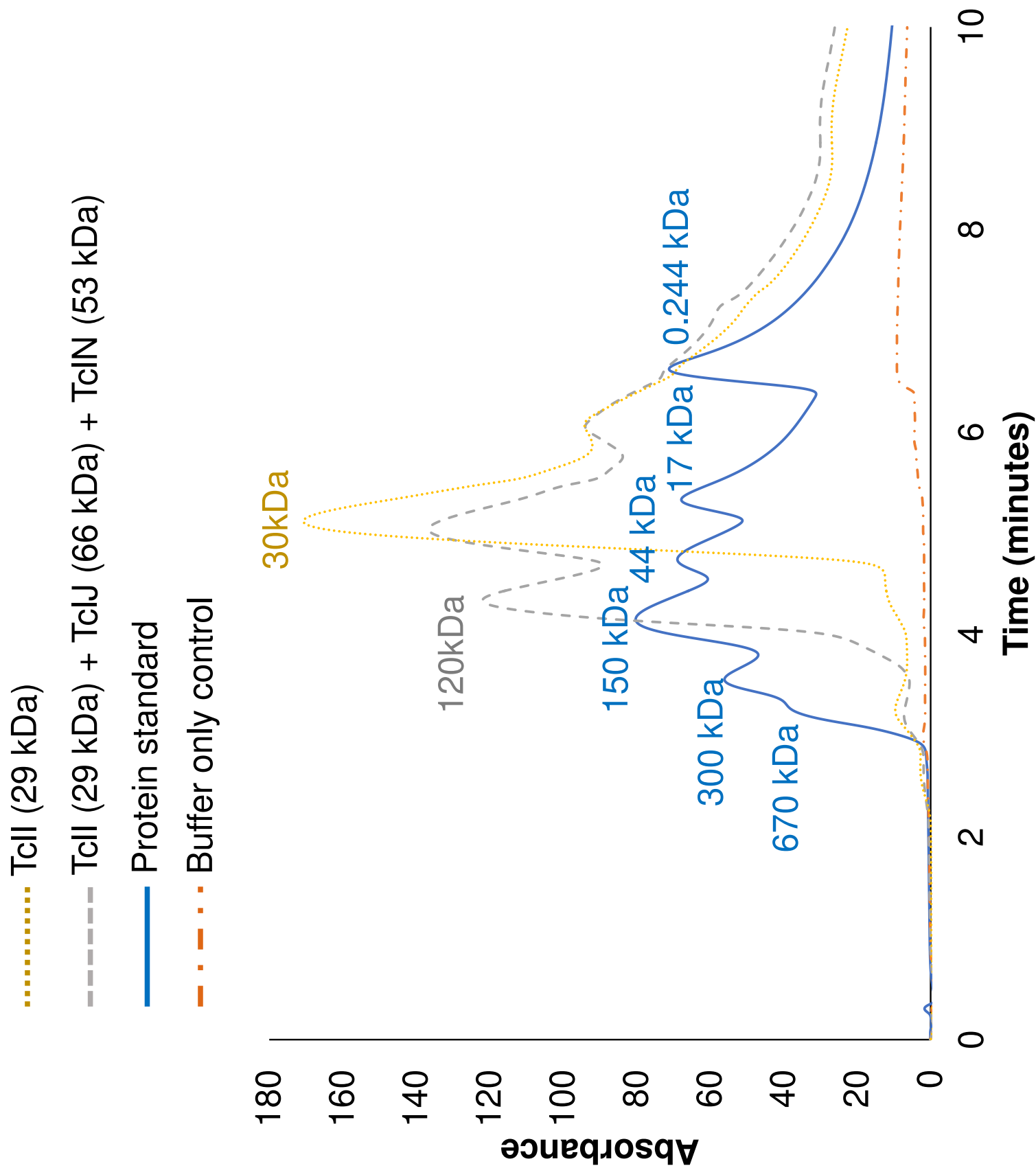
Lane 1: Vector only control

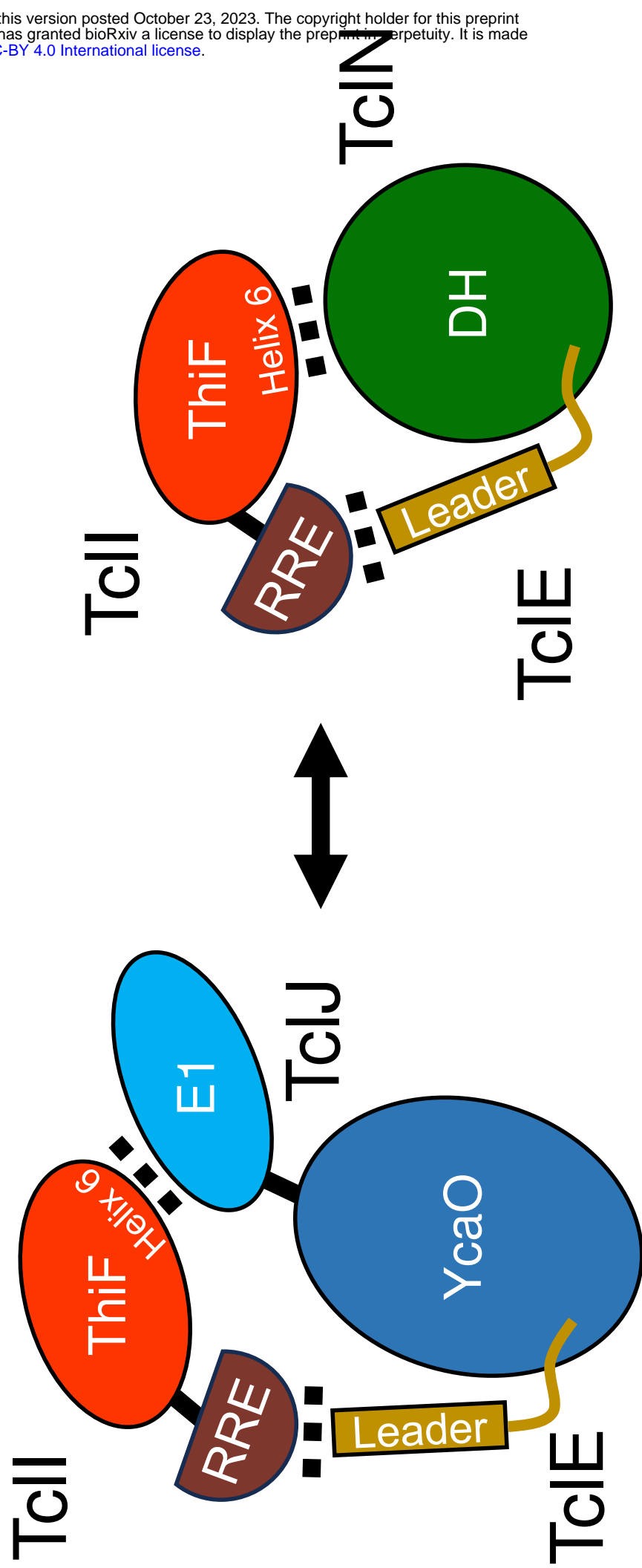
Lane 2: His<sub>6</sub> TcII

Lane 3: His<sub>6</sub> TcII TcIJ<sub>NTD1</sub>

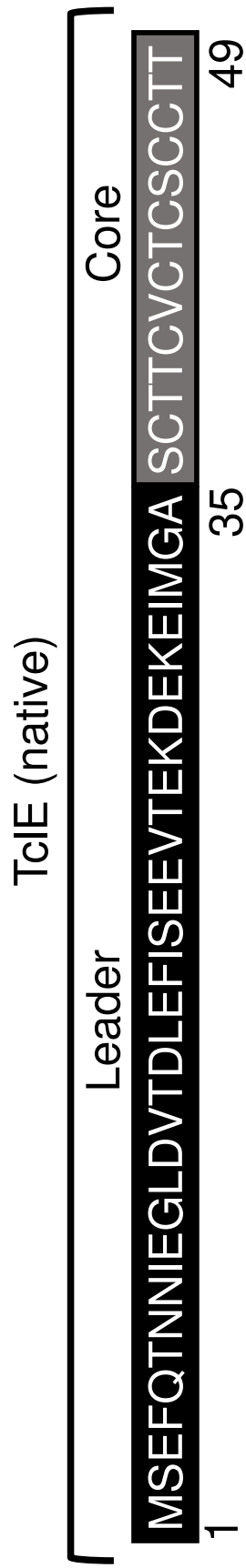
Lane 4: His<sub>6</sub> TcII TcIJ<sub>NTD2</sub>



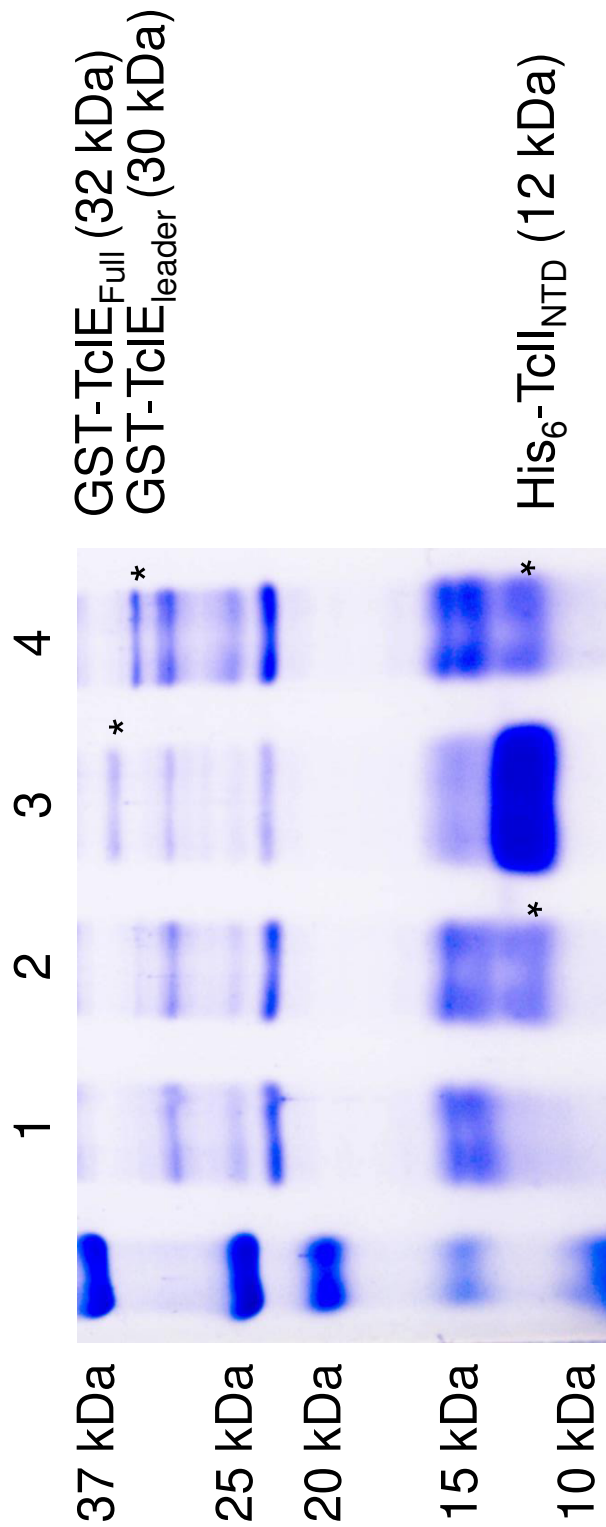


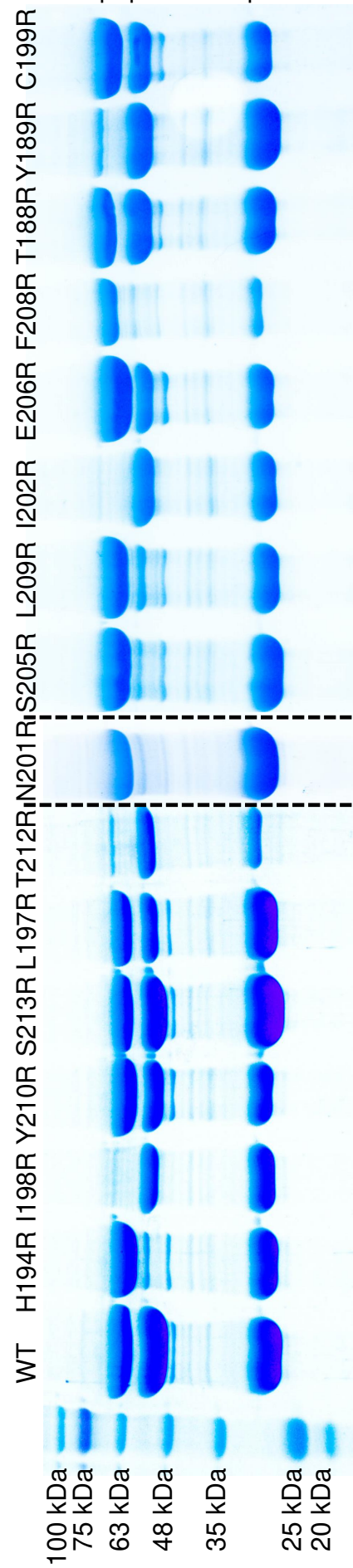


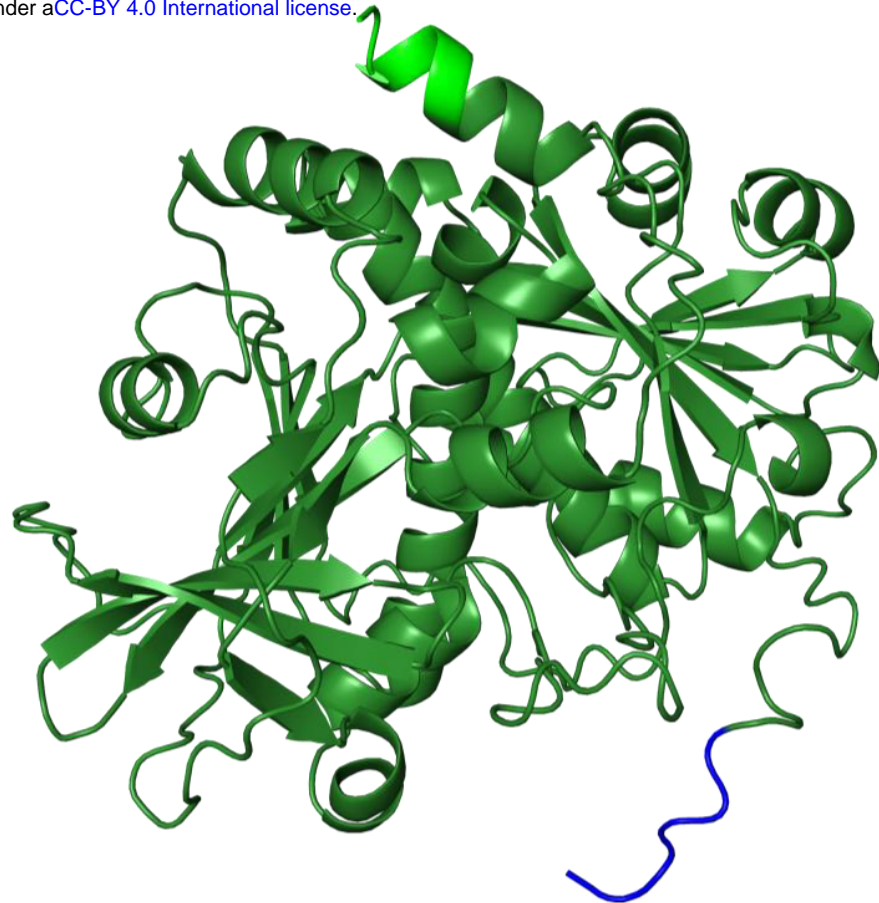




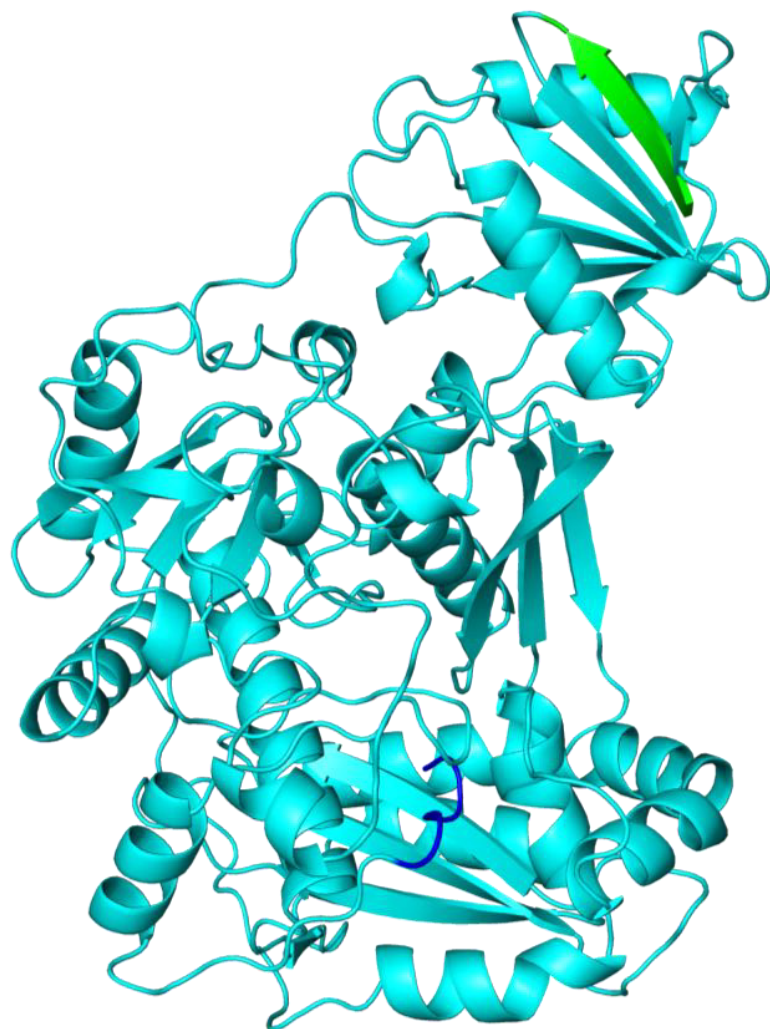
Lane 1: Vector only control







**B**



**A**

